INL/EXT-11-21817
Revision 1

Progress Report for Diffusion Welding of the NGNP Process Application Heat Exchangers

R. E. Mizia
D. E. Clark
M. V. Glazoff
T. E. Lister
T. L. Trowbridge

December 2011

Idaho National Laboratory

The INL is a U.S. Department of Energy National Laboratory
operated by Battelle Energy Alliance

DISCLAIMER

This information was prepared as an account of work sponsored by an agency of the U.S. Government. Neither the U.S. Government nor any agency thereof, nor any of their employees, makes any warranty, expressed or implied, or assumes any legal liability or responsibility for the accuracy, completeness, or usefulness, of any information, apparatus, product, or process disclosed, or represents that its use would not infringe privately owned rights. References herein to any specific commercial product, process, or service by trade name, trade mark, manufacturer, or otherwise, does not necessarily constitute or imply its endorsement, recommendation, or favoring by the U.S. Government or any agency thereof. The views and opinions of authors expressed herein do not necessarily state or reflect those of the U.S. Government or any agency thereof.

INL/EXT-11-21817
Revision 1

Progress Report for Diffusion Welding of the NGNP Process Application Heat Exchangers

R. E. Mizia, D. E. Clark, M. V. Glazoff, T. E. Lister, T. L. Trowbridge

December 2011

Idaho National Laboratory
Next Generation Nuclear Plant Project
Idaho Falls, Idaho 83415

Prepared for the
U.S. Department of Energy
Office of Nuclear Energy
Under DOE Idaho Operations Office
Contract DE-AC07-05ID14517

Next Generation Nuclear Plant Project

Progress Report for Diffusion Welding of the NGNP Process Application Heat Exchangers

INL/EXT-11-21817
Revision 1

December 2011

Approved by:

12/22/2011

Ronald Mizia
NGNP Materials Engineering

Date

12/22/11

Phil Mills
NGNP Engineering Director

Date

ABSTRACT

The U.S. Department of Energy selected the high temperature gas-cooled reactor as the basis for the Next Generation Nuclear Plant (NGNP). The NGNP will demonstrate the use of nuclear power for electricity, hydrogen production, and process heat applications. The NGNP Project is currently investigating the use of metallic, diffusion welded, compact heat exchangers to transfer heat from the primary (reactor side) heat transport system to the secondary heat transport system. An intermediate heat exchanger will transfer this heat to downstream applications such as hydrogen production, process heat, and electricity generation. The channeled plates that make up the heat transfer surfaces of the intermediate heat exchanger will have to be assembled into an array by diffusion welding. This report describes the preliminary results of a scoping study that evaluated the diffusion welding process parameters and the resultant mechanical properties of diffusion welded joints using Alloy 800H. The long-term goal of the program is to progress towards demonstration of small heat exchanger unit cells fabricated with diffusion welds. Demonstration through mechanical testing of the unit cells will support American Society of Mechanical Engineers' rules and standards development, reduce technical risk, and provide proof of concept for heat exchanger fabrication methods needed to deploy heat exchangers in several potential NGNP configurations.[1]

Researchers also evaluated the usefulness of modern thermodynamic and diffusion computational tools (*Thermo-Calc* and *Dictra*) in optimizing the parameters for diffusion welding of Alloy 800H. The modeling efforts suggested a temperature of 1150°C for 1 hour with an applied pressure of 5 MPa using 15 µm nickel foil as joint filler to reduce chromium oxidation on the welded surfaces. Good agreement between modeled and experimentally determined concentration gradients was achieved.

CONTENTS

ABSTRACT v

ACRONYMS xi

1. INTRODUCTION 1

2. EXPERIMENTAL TECHNIQUES AND SIMULATION METHODS 3
   - 2.1 Experimental Methods 3
     - 2.1.1 Sample Preparation and Characterization 3
     - 2.1.2 Gleeble Thermomechanical System for Diffusion Welding 3
     - 2.1.3 Optical Microscopy, Scanning Electron Microscopy, and Energy Dispersive X-ray Spectroscopy Analyses 5
   - 2.2 Simulation Methods 5
     - 2.2.1 Thermodynamic Modeling 5
     - 2.2.2 Diffusion Modeling 6
   - 2.3 Results and Discussion 6
     - 2.3.1 Test Matrix 6
     - 2.3.2 Mechanical Properties 11
     - 2.3.3 Diffusion Welding of Stacked Plates 13
     - 2.3.4 Scanning Electron Microscopy Results 21
     - 2.3.5 Scale-Up Issues 23
     - 2.3.6 Thermodynamic Modeling using *Thermo-Calc*© 24
     - 2.3.7 *Dictra* Modeling of the 800H/Ni/800H Diffusion Couple, Comparison to Experiment, and Optimization of Welding Conditions 29
   - 2.4 ASME Standards Development 31

3. SUMMARY 32

4. CONCLUSIONS 33

5. RECOMMENDATIONS 34

6. REFERENCES 35

FIGURES

Figure 1. Gleeble system: (a) General view of the Gleeble system with a specimen in it; (b) Gleeble system operation. 4

Figure 2. Diffusion welded sample of Alloy 800H. 5

Figure 3. Tensile test specimens. 11

Figure 4. Ultimate tensile strength results. 12

Figure 5. OPM images of 800H plate (A) as received and (B) after in-house finishing. 14

Figure 6. OPM images of 800H plate after externally contracted finishing (A) batch 1 and (B) batch 2. 15

Figure 7. OPM images of IN617 plate (A) as received and (B) after externally contracted finishing. Note larger image area for (A) when comparing. 15

Figure 8. OSU diffusion welding furnace and ram assembly. 16

Figure 9. Diffusion weld stack of 800H and end plates before welding. 16

Figure 10. Temperature record for tall stack (23 sheets). 17

Figure 11. Alloy 800H diffusion welded test blocks. 17

Figure 12. Test sample design. 18

Figure 13. Tensile samples from short stack. 19

Figure 14. Tensile samples from short stack. 19

Figure 15A. Low-magnification optical photomicrograph of two welds in the middle section of the taller stack. 20

Figure 15B. Higher-magnification optical photomicrograph of a weld in the middle section of the taller stack. 20

Figure 16. Diffusion weld bond line. 21

Figure 17. SEM chemical composition scan line – melted stack. 22

Figure 18. SEM chemical composition scan line – taller stack. 22

Figure 19. Phase composition of Alloys 800H as a function of temperature. 25

Figure 20. SEM image of an Alloy 800H sample heat treated at 1150°C for 3 hours and then quenched to room temperature. 26

Figure 21. Carbon-isopleth for Alloy 800H. 27

Figure 22. Iron-chromium phase diagram for Alloy 800H. 28

Figure 23. Chromium-isopleth for Alloy 800H. 28

Figure 24. Titanium-isopleth for Alloy 800H. 29

Figure 25. Comparison of model and experimental data (SEM/EDS analyses) for diffusion bonded specimen comprised of Alloy 800H (15 μm of nickel foil filler) and Alloy 800H. The duration of process was 3,600 sec at compressive pressure of 5 MPa and temperature 1150°C. *Dictra* modeling was done for the same conditions. 30

TABLES

Table 1. Chemical composition of Alloy 800H used in diffusion-welding experiments (given in wt%). 3

Table 2. 800H database scoping study of Table Y11215 (yellow shading denotes completed tests). 7

Table 3. Mechanical properties data. 13

Table 4. Roughness data for 800H plate; roughness values are in nanometers. 14

Table 5. Roughness data for IN617 plate. 15

Table 6. Mechanical properties data. 19

Table 7. Quantitative values for elemental analysis seen in Figure 16 and 17. 23

Table 8. Welding variables needed to qualify a welding procedure specification for diffusion welding. 31

ACRONYMS

ASME	American Society of Mechanical Engineers
B&PV	Boiler and Pressure Vessel
EDS	energy dispersive spectrometry
EDX	energy dispersive x-ray
HTGR	high temperature gas-cooled reactor
IHX	intermediate heat exchanger
INL	Idaho National Laboratory
NGNP	Next Generation Nuclear Plant
OPM	optical profile microscope
OSU	Oregon State University
RMS	root mean square
SEM	scanning electron microscope
VHTR	very high-temperature reactor
WDS	wavelength dispersive spectrometry

Progress Report for Diffusion Welding of the NGNP Process Application Heat Exchangers

1. INTRODUCTION

The U.S. Department of Energy selected a high temperature gas-cooled reactor (HTGR) as the basis for the Next Generation Nuclear Plant (NGNP). The NGNP Project will demonstrate the use of nuclear power to generate electricity, produce hydrogen, and provide process heat for other applications. The NGNP will be powered by a graphite moderated, helium cooled, prismatic or pebble bed, thermal neutron spectrum reactor that uses very high burnup, low-enriched uranium, tristructural-isotopic-coated fuel. The plant design will have a projected service life of 60 years. The plant size, reactor thermal power, and core configuration will ensure passive decay heat removal without fuel damage or radioactive material releases during accidents.

The basic technology for the NGNP was established in earlier HTGR plants, including DRAGON, Peach Bottom, Albeitsgemeinschaft Versuchsreaktor, Thorium Hochtemperatur Reaktor, and Fort St. Vrain. These reactor designs represent two design categories: the pebble bed modular reactor and the prismatic modular reactor. The Japanese High-Temperature Engineering Test Reactor and Chinese High-Temperature Reactor are currently demonstrating the feasibility of the reactor components and materials needed for a very high-temperature reactor (VHTR).

An important component of some VHTR designs is the intermediate heat exchanger (IHX) located in the heat transport system, which transfers heat from the primary heat transport system to the secondary heat transport system, which carries the heat to the downstream applications. The compact heat exchanger design concepts that will require the development of diffusion welding for the joining of plate stacks are:

- Printed-circuit heat exchanger
- Plate-fin heat exchanger
- Formed-plate heat exchanger
- Plate-machined heat exchanger
- Plate-stamped heat exchanger.

Diffusion welding of superalloys, including Alloy 800H, is a critical operation in the manufacture of components for the aerospace and nuclear industries.[1,2,3] It involves practically all of the phenomena studied by physical and mechanical metallurgy: control of grain growth and crystallographic texture across the weld interface; diffusion processes and phase transformations resulting in concentration profiles of different components and precipitates; and the prevention of high-temperature oxidation of different components (especially chromium). It is also necessary to optimize the welding temperature and the duration of exposure, applied compressive stress, heat-up schedule, and post-welding heat treatment. Even though solid-state diffusion is a relatively stable and predictable phenomenon, significant parameters are involved in the diffusion welding of real components in real alloys, and process development can require hundreds of expensive experiments, their mathematical planning, and the application of multiple linear regressions or artificial neural networks to achieve reliable results.[4]

The diffusion welding test program is described in Idaho National Laboratory (INL) PLN-3565.[5] The diffusion welds were made in a Gleeble Test System. The material of construction used in this test program is Alloy 800H, which is based on recommendations made in the NGNP Technology Development Roadmap.[6]

New software tools were applied to this program. During the last 15 years, powerful thermodynamic, diffusion, and finite element simulations (coupled to a new, state-of-the-art plasticity model) have come of age.[7,8,9,10,11,12] These computational tools—*Thermo-Calc* and *Dictra*—were used in the program to predict the metallurgical phases present in the diffusion welded joint at the diffusion welding temperature and at compact heat exchanger operating temperatures.

2. EXPERIMENTAL TECHNIQUES AND SIMULATION METHODS

2.1 Experimental Methods

2.1.1 Sample Preparation and Characterization

2.1.1.1 Material

The sample material, 0.5 in. diameter Alloy 800H round bar (UNS 80810/80811), for fabrication of the diffusion welded specimens was purchased to the requirements of ASTM International B408.[13] The chemical composition results of Huntington Alloys Corporation Heat (HH3507AR) are given in Table 1. In addition to alloying elements, a small amount (~0.001 wt%) of sulfur impurity was found.

Table 1. Chemical composition of Alloy 800H used in diffusion-welding experiments (given in wt%).

C	Mn	Fe	Si	Cu	Ni	Cr	Al	Ti	Co	N	Nb	S
0.08	1.02	45.57	0.31	0.18	32.16	19.59	0.46	0.55	0.08	0.007	0.053	0.001

2.1.1.2 Diffusion Weld Sample Preparation

The basic test procedure developed during the scoping studies involved the following process:

1. Prepare specimen ends with 600 or 800 grit grinding.
2. Prepare specimens further, as needed (e.g., nickel plating).
3. Weld thermocouple on one piece near interface.
4. Place mating parts in Gleeble jaws and manually adjust for alignment, including nickel interlayers (foils or plating) as appropriate.
5. Evacuate chamber to mid-10^{-4} Torr range (about 15 minutes).
6. Initiate Gleeble program, which applies force and heats to bonding temperature.
7. Manually fine-tune air ram pressure to maintain desired stress on specimen during bonding cycle (typically 3 hours).
8. Remove specimens after cooling.

2.1.2 Gleeble Thermomechanical System for Diffusion Welding

This diffusion welding investigation evaluated diffusion welding with no filler metal addition. It also evaluated filler metal additions to the faying (bonded) surfaces by the use of nickel plating, or a nickel foil interlayer as a filler material.

The diffusion bonds were performed using a Gleeble™ 3500 System,[a] a general-purpose servohydraulic thermomechanical testing device that can perform physical simulation of metallurgical processes as shown in Figure 1(a). The system can heat or cool specimens at rates up to 10,000°C/second and apply forces up to 20 tons at a rate of up to 1,000 mm/second. Figure 1(b) illustrates the operation of the Gleeble system for diffusion welding.

---

[a] Dynamic Systems, Inc., Poestenkill, New York.

(a) 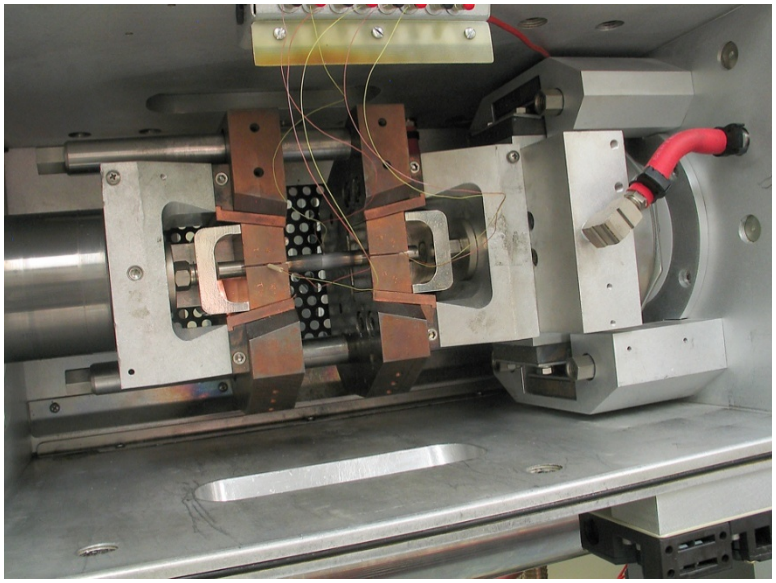

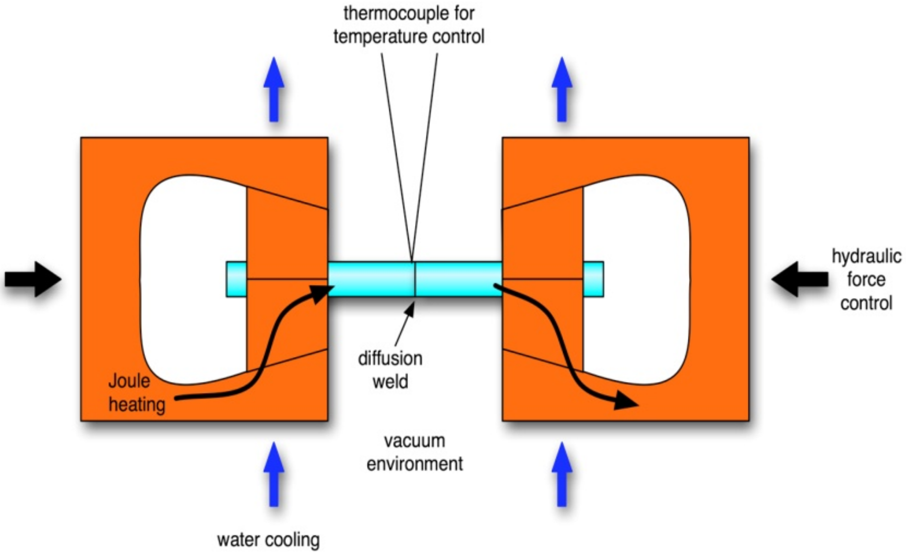
thermocouple for temperature control
hydraulic force control
Joule heating
diffusion weld
vacuum environment
water cooling

(b)

Figure 1. Gleeble system: (a) General view of the Gleeble system with a specimen in it; (b) Gleeble system operation.

Diffusion welding is a slow process with a relatively low applied stress that is well within the Gleeble's capacity, and the digital feedback loops are effective for precise control of the process. The Gleeble also provides a vacuum/controlled atmosphere chamber, which is required to control surface oxidation during the diffusion welding process. Heat is provided by Joule heating of the specimen held in water-cooled grips with feedback control provided by an attached thermocouple.

The Gleeble System is able to reproducibly create the thermal and mechanical components of the diffusion welding process. The Alloy 800H test material near the weld interface is exposed to the same thermal and mechanical history that it would see in the full-scale diffusion-welding process, which might be accomplished in a vacuum hot press or hot isostatic press. Figure 2 illustrates a diffusion welded sample from the Gleeble.

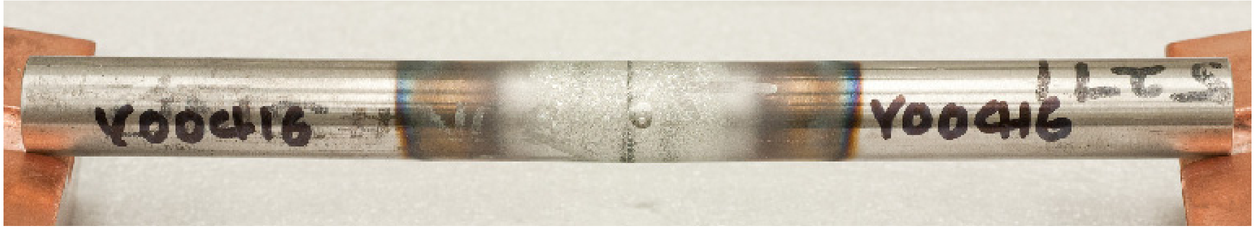

Figure 2. Diffusion welded sample of Alloy 800H.

2.1.2.1 Mechanical Properties Testing

Duplicate specimens were made for tensile testing, and a tensile specimen was designed nominally based on the ASTM International E-8 specimen.[14]

2.1.3 Optical Microscopy, Scanning Electron Microscopy, and Energy Dispersive X-ray Spectroscopy Analyses

Metallography was performed by taking a cylindrical section and slicing it longitudinally. One half was mounted and prepared for microstructural examination and the other half reserved for further testing, such as eventual exposure in the high temperature helium test loop.[15] Samples of diffusion bonded specimens were prepared for microstructural characterization using standard metallographic procedures, with a final polishing step of 0.04 µm silica in a vibratory polisher. Microstructures were developed for observation with a multistep etching process. The first step is an immersion in HCl (concentrated) for 5 to 10 seconds, followed by a methanol rinse, and a final step of immersion in a 2% bromine etchant (1 ml Br, 50 ml methanol) for 5 to 10 seconds.

Microstructural imaging was conducted by light optical microscopy and scanning electron microscopy (SEM) using both secondary electron hand backscattered electron imaging modes. The SEM analysis was conducted on a high resolution FEI Quanta 650 FEG™ SEM equipped with a field emission gun. This system is equipped with an EDAX™ Trident integrated materials characterization system which includes energy dispersive spectrometry (EDS), electron backscattered diffraction, and wavelength dispersive spectrometry (WDS) capabilities. For the chemical analysis used in this investigation, EDS is considered a semiquantitative technique and WDS is considered a quantitative technique. The SEM imaging and WDS elemental analysis were performed at an accelerating voltage of 20 kV.

2.2 Simulation Methods

2.2.1 Thermodynamic Modeling

The construction of isopleths and initial assessment of thermodynamic equilibrium to establish phase composition of the Alloy 800H was done using *Thermo-Calc* Classic (Version S). A detailed description of thermodynamic models and optimization algorithms used to establish the equilibrium compositions of alloys can be found in the *Thermo-Calc* manual.[16] A broad exposition of modern thermodynamics behind the *Thermo-Calc* computational platform is given by Hillert.[8] Commercial *Thermo-Calc* databases TTFE6 (iron-based) and TTNI8 (nickel-based) were used in all equilibrium calculations. Alloy 800H contains approximately 46 wt% iron and 32 wt% nickel, and the application of either database yielded practically identical results, indicating the robustness of both databases. The calculation of a single equilibrium for Alloy 800H, comprising 12 components and an impurity (sulfur), took no more than 2 to 3 seconds on a PC-based workstation. Calculations for the different isopleths, constructed to probe phase fields and establish the optimal temperature of the diffusion welding process, took from 180 up to ~2,000 seconds of CPU time, on average. In addition to thermodynamic and phase field considerations, it is necessary to take into account the possibility of creep at elevated temperatures as well as to achieve the relatively large grain size in 800H necessary to effectively control creep. Only phase diagrams and thermodynamic factors are discussed at this point.

2.2.2 Diffusion Modeling

Diffusion modeling was conducted using *Dictra* Version 25 software—a "sister" program of *Thermo-Calc* that can solve numerous metallurgical problems, as indicated in the *Dictra* Manual.[17] It allows the exploration of diffusion-controlled phase transformations, including such phenomena as diffusion couples, both single-phase and heterogeneous. In the latter case, it is assumed that the volume fraction of the second phase (e.g., the γ' strengthening precipitates or the equilibrium carbide TiC constituent particles in Alloy 800H) is small. Additionally, it is assumed that the average concentration in the strengthening phase is defined by the conditions of local equilibrium for the average concentrations of components.[17,18] Additional explanations and comments to these problems and the methods of their solution can be found in a review by Borgenstam et al.[18]

Given the complexity of the Alloy 800H system, changes in the titanium-niobium carbonitride[b] distribution across the welded joint were ignored since the titanium and niobium carbides, nitrides, and carbonitrides are quite stable. These phases form and dissolve only at temperatures near Alloy 800H's melting range (>1360°C), and are thus features of the alloy base metal that are little affected by diffusion welding in the vicinity of 1150°C. The concentration profiles of the major chemical elements were considered.

The modeled system comprised a 50 μm rectangle of Alloy 800H followed by a 15 μm layer of pure nickel filler metal across the diffusion welded joint followed by another 50 μm rectangle of 800H. The nickel layer (which may be considered a filler metal) was used because it helped suppress the chromium oxidation process at the faying surface interface, and improved the mating of the welded parts, both of which improve the quality of the welded joint. Nickel plating is an alternative method of applying an interlayer. A nonuniform mesh (option "Double-Geometric" in *Dictra*) was used with the corresponding factor of 0.98 for both interfaces. This helped introduce more discretized points across the boundaries, where the chemical potential gradients were high, and fewer points far from the weld. The initial concentration of all components, except nickel, which was considered a dependent component, was modeled using two Heaviside functions for each chemical element. For example, in the case of chromium, the following expression was used as the initial condition for diffusion process simulation: C_{Cr} = 1.0e-6 + 0.1959 * *hs* (50e-6 – x) + 0.1959 * *hs* (x - 65*e-6). In this expression, 0.1959 is the bulk chromium concentration (weight-fraction) in the Alloy 800H; 1.0e-6 = 10^{-6} plays the role of "zero" (a very small number); 15 μm = 65 μm - 50 μm is the width of the nickel interconnect, *x* stands for the current distance, and "*hs*" stands for the Heaviside function. To overcome numerical instabilities of integration, a fully-implicit Euler integration method offered in *Dictra* as an option, was used. A calculation simulating diffusion welding process for 1 hour (3,600 seconds) at 1150°C (the optimal conditions that have been established), took, on average, about 4 hours to complete a simulation run.

2.3 Results and Discussion

2.3.1 Test Matrix

The scoping test matrix and test completion data is shown in Table 2, which defines the progress of all tests from 1 through 75.

---

[b] $(Ti_{1-x}Nb_x)(C,N)$, according to the results of equilibrium calculations at 1150°C.

Table 2. 800H database scoping study of Table Y11215 (yellow shading denotes completed tests).

		Surface Condition: Ground to 600 Grit		Bonding Geometry			Bonding Parameters			Analysis	
Sequence	**Specimen (Date Code)**	**Ni Plated (per side)**	**Ni Foil**	**Number of Bonds**	**Base Material**	**Inserted Material**	**Time (hours)**	**Temp. (°C)**	**Stress (MPa)**	**UTS (MPa if Tested)**	**He Loop Exposure**
1	X91215	No	No	1	800H	—	2	1050	2.77±1.90	Met. Mount	—
2	X91223	No	No	1	800H	—	3	1100	6.02±0.34	Met. Mount	—
3	Y00107	No	No	1	800H	—	3	1150	—	Met. Mount	Intended
4	Y00108	No	No	1	800H	—	—	—	—	—	—
5	Y00111	~1 µm	No	1	800H	—	3	1150	5.45±2.91	Met. Mount	—
6	Y00126	No	15 µm	1	800H	—	3	1150	7.36±1.24	Met. Mount	—
7	Y00127	~1 µm	No	1	800H	—	3	1150	6.07±0.61	537.2	—
8	Y00128	No	No	1	800H	—	3	1150	5.72±1.38	180.0	—
9	Y00223	No	15 µm	1	800H	—	3	1150	6.92±0.53	526.7	—
10	Y00407	No	No	1	800H	—	3	1150	10.35±0.54	Met. Mount	Run 25
11	Y00408A	No	No	2	800H	Alloy X	3	1150	6.22±0.90	Met. Mount	Run 25
12	Y00408B	No	15 µm	2	800H	Alloy X	3	1150	4.26±1.00	Met. Mount	Run 25
13	Y00414	No	No	1	800H	—	3	1150	4.38±0.92	466.0	—
14	Y00415A	~1 µm	No	1	800H	—	3	1150	4.72±1.00	537.0	—
15	Y00415B	~1 µm	No	1	800H	—	3	1150	5.08±0.59	531.0	—
16	Y00416	No	No	1	800H	—	3	1150	4.73±0.46	536.0	—
17	Y00427A	No	No	1	800H	—	—	—	—	—	—
18	Y00427B	No	No	1	800H	—	3	1150	5.26±1.56	187.1	—
19	Y00428	No	15 µm	1	800H	—	3	1150	5.07±1.61	560.9	—
20	Y00511	No	15 µm	1	800H	—	3	1150	5.45±1.50	559.2	—
21	Y00513	No	No	1	800H	—	3	1150	4.71±1.42	333.3	—
22	Y00517	No	No	3	800H	800H	3	1150	4.34±1.34	Met. Mount	Intended
23	Y00520	No	15 µm	3	800H	800H	3	1150	5.15±0.94	Met. Mount	Intended
24	Y00527	No	15 µm	1	800H	—	1.5	1150	4.35±1.05	Met. Mount	Intended

Table 2. (continued).

		Surface Condition: Ground to 600 Grit		**Bonding Geometry**			**Bonding Parameters**			**Analysis**	
Sequence	**Specimen (Date Code)**	**Ni Plated (per side)**	**Ni Foil**	**Number of Bonds**	**Base Material**	**Inserted Material**	**Time (hours)**	**Temp. (°C)**	**Stress (MPa)**	**UTS (MPa if Tested)**	**He Loop Exposure**
Future scoping work: Effects of bonding time											
25	Y00802A	~1 µm	No	1	800H	—	1	1150	6.07±0.63	Met. Mount	Run 31
26	Y01118	~1 µm	No	1	800H	—	2	1150	5.54±0.73	Not Mounted	Intended
27	Y01213	~1 µm	No	1	800H	—	5	1150	5.07±1.57	Not Mounted	Intended
28	Y00803	~1 µm	No	1	800H	—	7	1150	5.23±0.99	Met. Mount	Run 31
29	Y00804A	No	15 µm	1	800H	—	1	1150	5.25±0.66	Met. Mount	Run 31
30	Y00804B	No	15 µm	1	800H	—	2	1150	5.27±1.06	Met. Mount	Run 31
31	Y01005	No	15 µm	1	800H	—	5	1150	5.02±2.10	Met. Mount	Run 31
32	Y01007	No	15 µm	1	800H	—	7	1150	4.91±1.22	Not Mounted	Intended
33	Y00802B	~1 µm	No	1	800H	—	1	1150	5.29±0.33	532.9	No
34	TBD	Yes	No	1	800H	—	2	1150	5 Nom.	Tensile	—
35	TBD	Yes	No	1	800H	—	5	1150	5 Nom.	Tensile	—
36	TBD	Yes	No	1	800H	—	7	1150	5 Nom.	Tensile	—
37	TBD	No	Yes	1	800H	—	1	1150	5 Nom.	Tensile	—
38	Y01004	No	15 µm	1	800H	—	2	1150	4.96±1.29	554.7	No
39	Y00812	No	15 µm	1	800H	—	5	1150	5 Nom.	536.9	No
40	Y01006	No	15 µm	1	800H	—	7	1150	5 Nom.	Not Tested	—
41	TBD	Yes	No	1	800H	—	1	1150	5 Nom.	Tensile	—
42	TBD	Yes	No	1	800H	—	2	1150	5 Nom.	Tensile	—
43	TBD	Yes	No	1	800H	—	5	1150	5 Nom.	Tensile	—
44	TBD	Yes	No	1	800H	—	7	1150	5 Nom.	Tensile	—
45	TBD	No	Yes	1	800H	—	1	1150	5 Nom.	Tensile	—
46	TBD	No	Yes	1	800H	—	2	1150	5 Nom.	Tensile	—
47	TBD	No	Yes	1	800H	—	5	1150	5 Nom.	Tensile	—
48	TBD	No	Yes	1	800H	—	7	1150	5 Nom.	Tensile	—

Table 2. (continued).

		Surface Condition: Ground to 600 Grit		Bonding Geometry			Bonding Parameters			Analysis	
Sequence	Specimen (Date Code)	Ni Plated (per side)	Ni Foil	Number of Bonds	Base Material	Inserted Material	Time (hours)	Temp. (°C)	Stress (MPa)	UTS (MPa if Tested)	He Loop Exposure
Effects of multiple layers, similar to printed circuit heat exchanger geometry											
49	TBD	Yes	No	2	800H	800H	3	1150	5 Nom.	Met. Mount	Intended
50	TBD	Yes	No	2	800H	800H	3	1150	5 Nom.	Tensile	—
51	TBD	Yes	No	2	800H	800H	3	1150	5 Nom.	Tensile	—
52	TBD	Yes	No	3	800H	800H	3	1150	5 Nom.	Met. Mount	Intended
53	TBD	Yes	No	3	800H	800H	3	1150	5 Nom.	Tensile	—
54	TBD	Yes	No	3	800H	800H	3	1150	5 Nom.	Tensile	—
55	TBD	No	Yes	2	800H	800H	3	1150	5 Nom.	Met. Mount	Intended
56	TBD	No	Yes	2	800H	800H	3	1150	5 Nom.	Tensile	—
57	TBD	No	Yes	2	800H	800H	3	1150	5 Nom.	Tensile	—
58	TBD	No	Yes	3	800H	800H	3	1150	5 Nom.	Met. Mount	Intended
59	TBD	No	Yes	3	800H	800H	3	1150	5 Nom.	Tensile	—
60	TBD	No	Yes	3	800H	800H	3	1150	5 Nom.	Tensile	—
Use of larger diameter materials											
61	TBD	Yes	No	2	800H	800H	3	1150	5 Nom.	Met. Mount	Intended
62	TBD	Yes	No	2	800H	800H	3	1150	5 Nom.	Tensile	—
63	TBD	Yes	No	2	800H	800H	3	1150	5 Nom.	Tensile	—
64	TBD	Yes	No	3	800H	800H	3	1150	5 Nom.	Met. Mount	Intended
65	TBD	Yes	No	3	800H	800H	3	1150	5 Nom.	Tensile	—
66	TBD	Yes	No	3	800H	800H	3	1150	5 Nom.	Tensile	—
67	Y01027	No	15 µm	1	800H	1.0 inch	3	1150	4.51±0.51	Met. Mount	Intended
68	TBD	No	Yes	2	800H	800H	3	1150	5 Nom.	Tensile	—
69	TBD	No	Yes	2	800H	800H	3	1150	5 Nom.	Tensile	—
70	Y01029	No	5 µm	1	800H	0.75 inch	3	1150	5.07±0.40	Not Mounted	Intended
71	TBD	No	Yes	3	800H	800H	3	1150	5 Nom.	Tensile	—
72	TBD	No	Yes	3	800H	800H	3	1150	5 Nom.	Tensile	—

Table 2. (continued).

Sequence	Specimen (Date Code)	Surface Condition: Ground to 600 Grit		Bonding Geometry			Bonding Parameters			Analysis	He Loop Exposure
		Ni Plated (per side)	Ni Foil	Number of Bonds	Base Material	Inserted Material	Time (hours)	Temp. (°C)	Stress (MPa)	UTS (MPa if Tested)	
Miscellaneous tests in addition to original matrix											
73	Y00720A	~1 μm	No	1	800H	—	1.5	1150	5.25±0.92	548.5	No
74	Y00720B	~1 μm	No	1	800H	—	1.5	1150	5.02±0.57	549.5	No
75	Y10113	~1 μm	No	1	800H	—	3	1150	5.02±0.58	Not Tested	—

The nominal welding parameters for these tests were a temperature of 1150°C, 5 MPa applied stress, and 3-hour hold time under a vacuum of about 5×10^{-4} Torr. As will be discussed later, the thermodynamic and kinetic modeling effort suggested that a time of 1-hour at these same parameters would be sufficient. Although the 3-hour time proved to be effective, the modeling indicated that shorter times, on the order of 1-hour, might also be sufficient. This would have an advantage in reducing overall creep and in productivity. It might also be that a relatively short time under compressive load followed by a much longer time at elevated temperature (a post-weld heat treatment) would be beneficial.

2.3.2 Mechanical Properties

Figure 3 shows (1) the as-tested tensile bars of an alloy bar in the as-received condition along with diffusion welded samples of alloy 800H prepared with the following bond interface preparation: (2) nickel electroplate 1 µm thick on each mating surface, (3) interface of 15 µm nickel foil placed between 600 grit ground mating surfaces, and (4) mating surfaces ground to a 600 grit finish, As can be seen in Figure 4, the ultimate tensile strength of bonds using filler metal (nickel plate or foil) is typically near that of the base metal. The only specimens showing reduced strengths are those made with ground surfaces that had no added filler metal.

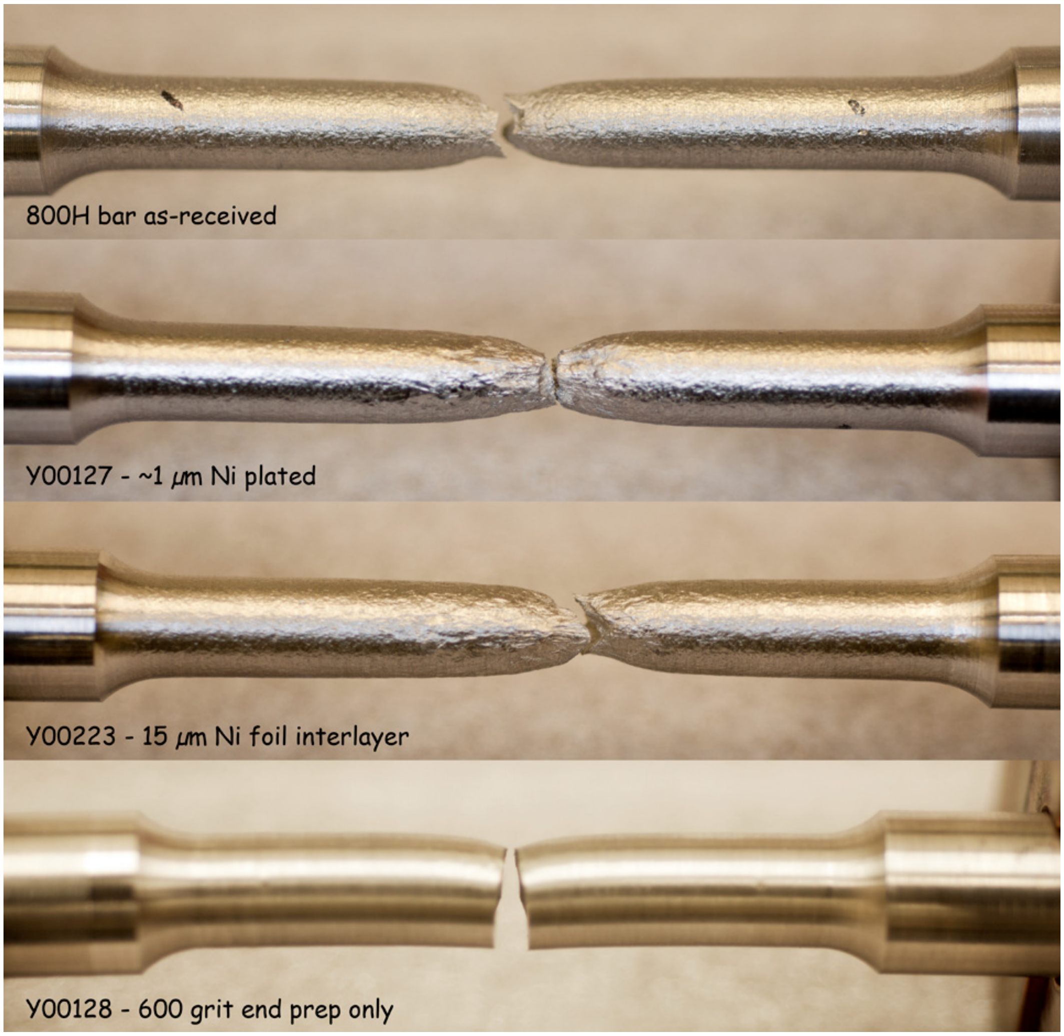
800H bar as-received
Y00127 - ~1 µm Ni plated
Y00223 - 15 µm Ni foil interlayer
Y00128 - 600 grit end prep only

Figure 3. Tensile test specimens.

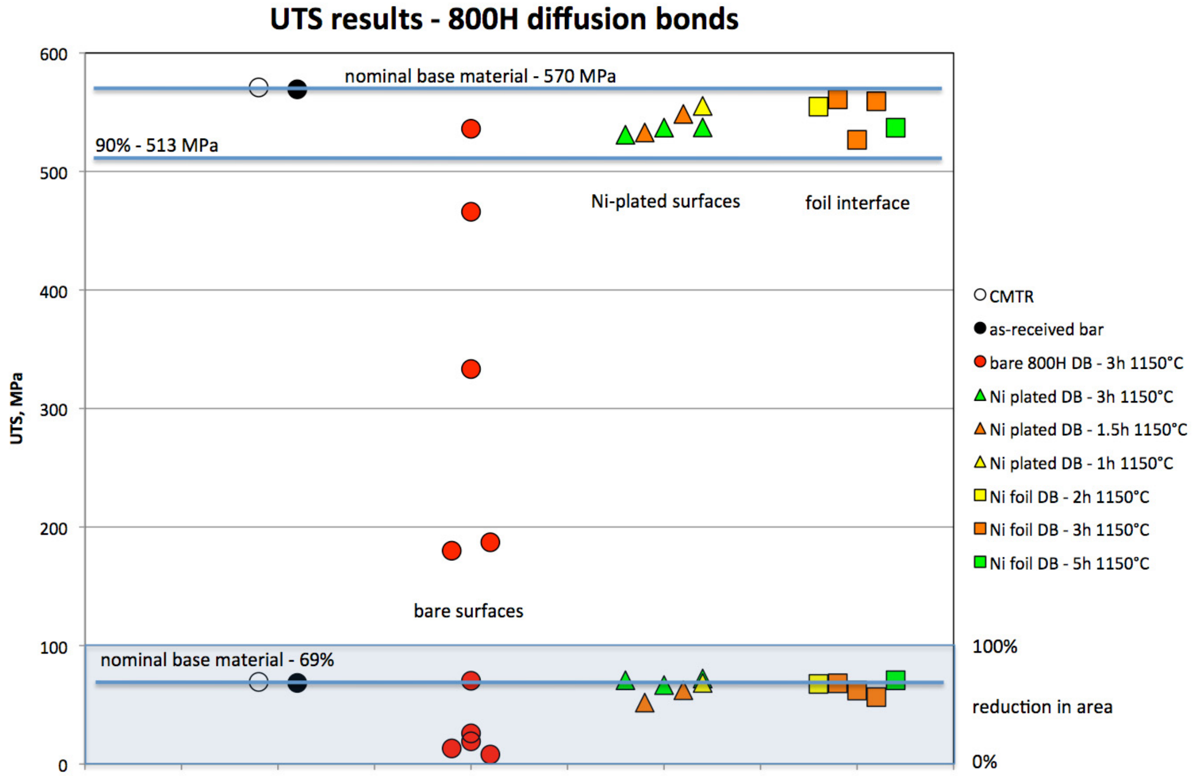

Figure 4. Ultimate tensile strength results.

Various diffusion welded alloy 800H specimens were tensile tested per the requirements of ASTM International E8[13] with the results shown in Table 3 and plotted in Figure 4. As-received specimens were machined out of the 0.5 in. round bar. All samples were ground though a 600 or 800 grit surface finish on the bonding (faying) surfaces. Added filler metal of pure nickel were also investigated. Some samples had an electrodeposited nickel layer of about 1µm on both bonding surfaces. Other welds used a 15 µm thick nickel foil placed between the 600 grit finished surfaces. The optimized welding parameters were found to be 1150°C for 3 hours, with approximately 5 MPa of applied compressive stress. This was based on metallographic examination of the initial welds and on the experience of previous diffusion bonding of Alloy 617. Earlier work (not shown here) ,using lower temperatures and times, produced insufficient bonding in the specimens examined by metallography. Stresses of 3 to 5 MPa were chosen also based on Alloy 617 experience and observations that a stress of 10 MPa causes macroscale creep deformation.

The ultimate tensile strength of specimens fabricated with either nickel-plating or a nickel interlayer is typically near that of the base metal. The specimens showing reduced strengths were made with ground surfaces (no nickel plating or nickel interlayer). This reduced strength may be caused by alignment problems with some of the specimens. These specimens fractured at the bond line with evidence of heat tinting, indicating that the specimen was heated while the interface was not bonding in those areas, and residual gases in the vacuum chamber were able to oxidize the surface. The one specimen without a filler metal addition that exhibited good properties was given an overnight pump-down in the Gleeble System vacuum chamber. This measurement should be repeated in additional testing. Ni foil or Ni plating can increase part conformance and protect from oxidation during heating; ground faying surfaces might not conform where pressures are low to avoid creep at the bonding temperature.

Table 3. Mechanical properties data.

Sample	Interface	Time (hours)	Temp. (°C)	Bond Stress (MPa)	YS (MPa)	UTS (MPa)	RA (%)
800H-SMC (CMTR* data)	—	—	—	—	238.6	570.9	69.3
800H-AR (INL analysis)	—	—	—	—	220.0	569.3	64.4
Y00126	Ground, 600 grit,15 µm Ni foil	3	1150	7.00	—	—	—
Y00127	Ground, 600 grit, Ni plated ~1 µm on each surface	3	1150	6.04	178.0	537.2	69.7
Y00128	Ground, 600 grit	3	1150	5.93	<180	180.0	12.9
Y00223	Ground, 600 grit, 15 µm Ni foil	3	1150	6.00	178.0	526.7	62.3
Y00414	Ground,800 grit	3	1150	4.38	—	466	25.9
Y00415A	Ground, 600 grit, Ni-plate	3	1150	4.72	—	537	66.6
Y00415B	Ground, 600 grit, Ni-plate	3	1150	5.08	—	531.0	70.7
Y00416	Ground,800 grit, overnight vacuum	3	1150	4.73	—	536	70.3
Y00427B	Ground,800 grit	3	1150	5.26	—	187.1	8.0
Y00428	Ground, 800 grit, 15µ Ni foil	3	1150		—	560.9	68.1
Y00511	Ground, 800 grit, 15µ Ni foil	3	1150	5.45	—	559.2	56.5
Y00513	Ground, 800 grit	3	1150	4.71	—	333.3	19.2
Y00720A	Ground, 600 grit, Ni plate	1.5	1150	5.25	—	548.5	62.3
Y00720B	Ground, 600 grit, Ni plate	1.5	1150	5.02	—	549.5	51.8
Y00802B	Ground, 600 grit, Ni plate	1	1150	5.29	—	539.2	68.4
Y00812	Ground, 600 grit, 15µ Ni foil	5	1150	5 (nom)	—	536.9	70.7
Y01004	Ground, 600 grit, 15µ Ni foil	2	1150	4.96	—	554.7	67.6

---

* Certified Material Test Report

2.3.3 Diffusion Welding of Stacked Plates

2.3.3.1 Surface Finish of Plate or Sheet Material for Diffusion Welding

The plate or sheet material specifications for nickel alloys does not have adequate surface finish requirements for diffusion welding of stacks of sheet or plate material. The as-received nickel alloy plate material has a matte rather than a ground appearance. Flat surfaces should be used to provide an ideal bonding surface where maximum diffusion can occur. Surfaces were characterized for surface finish quality using an optical profile microscope (OPM). This instrument provides a 3-D map of the surface texture and has software roughness calculations based on the data maps. The smaller the numerical value (in root mean square, RMS) the smoother the surface texture. Figure 5A provides an OPM image of an 8 × 8 in. 800H plate before finishing. Note that the bar at the right side of each image is a key for relative surface height. The uniform green color of the as received finish indicates a mostly flat surface. However, pits (blue regions) up to 15 mm deep exist in the surface. Table 4 shows roughness data for 800H plates. While the INL is well equipped to polished small specimens, facilities to polish larger plates are limited. A dual orbital (DA) sander with 50 grit paper (coarse) was used to remove material. Progressively, finer grits were then used to smooth the surface (600 grit the final grade). This produced the image shown in Figure 5B. While this reduced the depth of pits, which reduced the RMS roughness, this process was time consuming and deemed an unworkable solution. To provide a smooth surface, a more efficient method of material removal was needed.

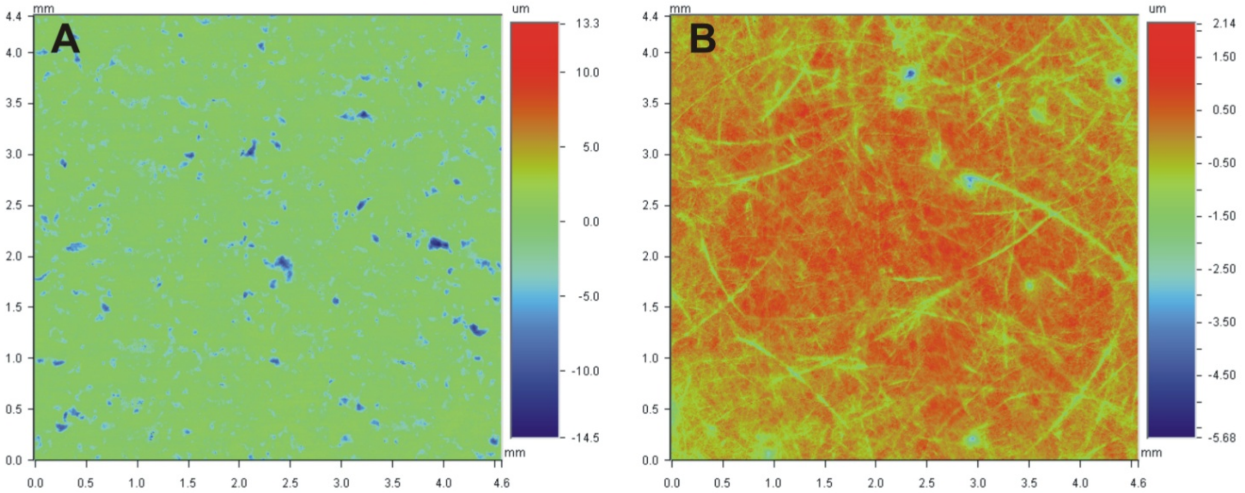

Figure 5. OPM images of 800H plate (A) as received and (B) after in-house finishing.

Table 4. Roughness data for 800H plate; roughness values are in nanometers.

	As Received	50 Grit Up DA	Harrison Polish Batch 1	Harrison Polish Batch 2 Plate #1	Harrison Polish Batch 2 Plate #2
1	957.88	336.31	97.04	115.72	267.39
2		308.81	88.17	120.48	194.18
3		347.31	110.09	124.52	200.
Avg	957.88	330.81	98.43	120.24	220.57
Pits	Numerous, deep	Less, shallow	Rare, minute	Less, shallow	Less, shallow

To produce a higher quality surface finish, three 800H plates were sent to Harrison Metals Inc. in Houston, TX to remove a more substantial depth of material and then polish to a 600 grit finish. The returned plates showed a high quality finish. OPM was performed on one plate as shown in Figure 6A. The plates from this initial batch proved to be very smooth, with RMS roughness below 100 nm (see Table 4). The analyzed plate did not reveal signs of previous pitting. After receiving this test batch the remaining plates were sent for finishing. Two plates were analyzed by OPM (Figures 7A and 7B) and did not show the level of smoothness obtained from the initial batch (Figure 6B and Table 4). The surface showed signs of the previously existing surface pits. This indicates that sufficient material was not removed during this process. While one of the plates was similar in RMS roughness, the second plate was over twice as rough as the plate analyzed from the first batch as shown in Table 5. This is likely because of inconsistent surface treatment of each piece. It is recommended that surface quality acceptance criteria be established to prevent this issue in future work.

Poor surface finish was also observed with IN617 plates. These pits appeared more numerous but smaller in area and somewhat less deep (~10 mm). Images of IN617 before and after contracted finishing are shown in Figure 7. Tabulated roughness data is shown in Table 5. The RMS roughness was decreased by about 50% after finishing. The roughness appears to be the same issue observed for the second 800H batch: insufficient removal of material. Thus existing pits remained in the surface.

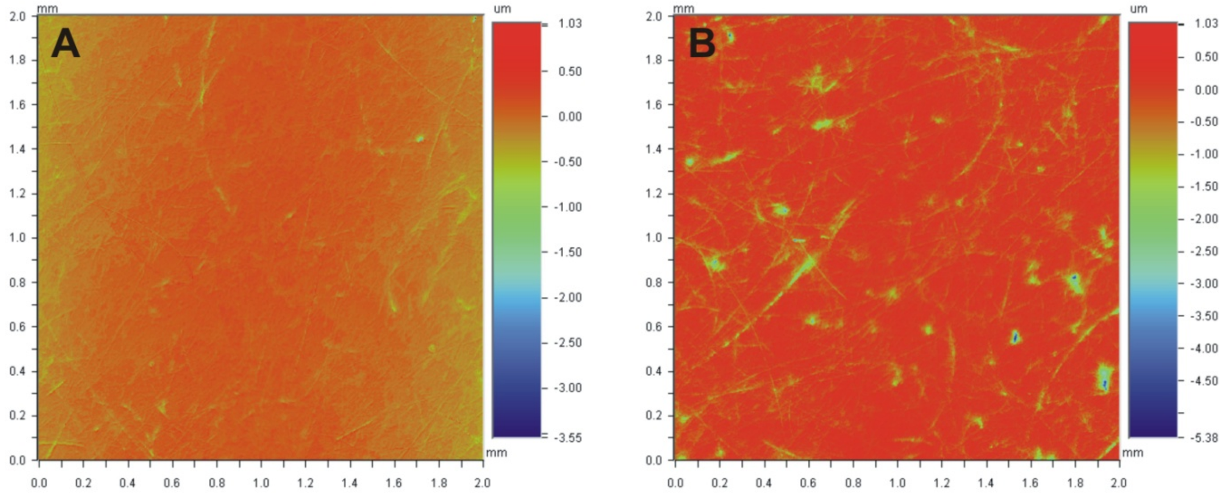
A
B
mm
um
2.0
1.8
1.6
1.4
1.2
1.0
0.8
0.6
0.4
0.2
0.0
1.03
0.50
0.00
-0.50
-1.00
-1.50
-2.00
-2.50
-3.00
-3.50
-4.00
-4.50
-3.55
-5.38

Figure 6. OPM images of 800H plate after externally contracted finishing (A) batch 1 and (B) batch 2.

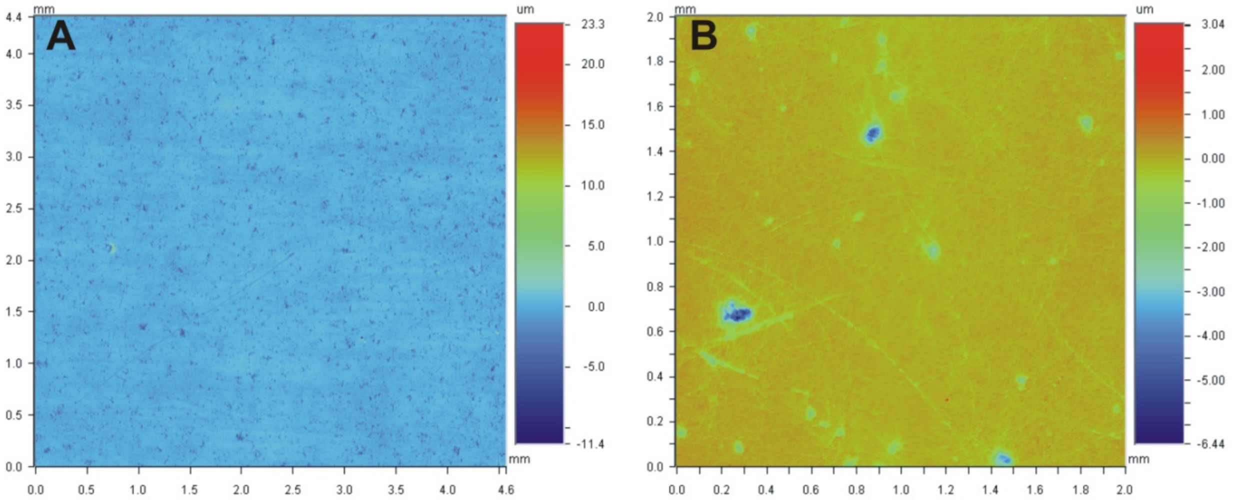
A
B
mm
um
4.4
4.0
3.5
3.0
2.5
2.0
1.5
1.0
0.5
0.0
4.6
23.3
20.0
15.0
10.0
5.0
0.0
-5.0
-11.4
3.04
2.00
1.00
0.00
-1.00
-2.00
-3.00
-4.00
-5.00
-6.44

Figure 7. OPM images of IN617 plate (A) as received and (B) after externally contracted finishing. Note larger image area for (A) when comparing.

Table 5. Roughness data for IN617 plate.

	As Received	Harrison Polish Plate #1	Harrison Polish Plate #2
1	4 .96	273.36	119.11
2	443.96	223.49	132.92
3	452.77	149.55	147.19
Avg	436.90	215.47	133.07
Pits?	Numerous, deep	Less, shallow	Less, shallow

2.3.3.2 Diffusion Welding at Oregon State University

The NGNP Engineering diffusion welding development effort has progressed from the welding of small bars in the Gleeble system to welding of stacked, thin-gage plates that will better represent the compact heat exchanger design. The first round of diffusion welding of 2.1-in.-square stacks of 1/16 in. thick 800H material has been recently completed at Oregon State University (OSU). OSU was chosen to perform this work because of their experience with the diffusion welding of similar stacks for fluid dynamics applications with their vacuum hot press

The OSU vacuum hot press shown in Figure 8 contains graphite resistance heating elements in a furnace shell that slides down over the specimen and connects to a turbomolecular-pumped high vacuum system. The arrangement of the 800H diffusion welding stack shown in Figure 9 consists of two 1/2 in. plates of 800H material sandwiching many 1/16 in. sheets of 800H. Graphite blocks about 5/8 in. thick serve to spread the load of the cylindrical graphite rams over the surface of the 800H plates. Interfaces not intended for bonding (graphite/graphite and graphite/metal) are lightly coated with boron nitride. Control thermocouples are arranged in contact with the stack near its vertical center, and additional thermocouples monitor thermal gradients. The stack of alloy 800H plates and alloy 800H end blocks (before diffusion welding) is shown in Figure 9.

Three alloy 800H stacks were welded. The first stack (16 sheets between two 1/2 in. 800H plates) overheated and partially melted on one end because control misplaced thermocouples were misplaced in the vertical direction. The subsequent two stacks (one with 16 sheets between two 1/2 in. 800H plates, the other with 23 sheets between two 1/2 in. 800H plates) followed nominal process parameters. Figure 10 shows the temperature record for the 23-sheet stack.

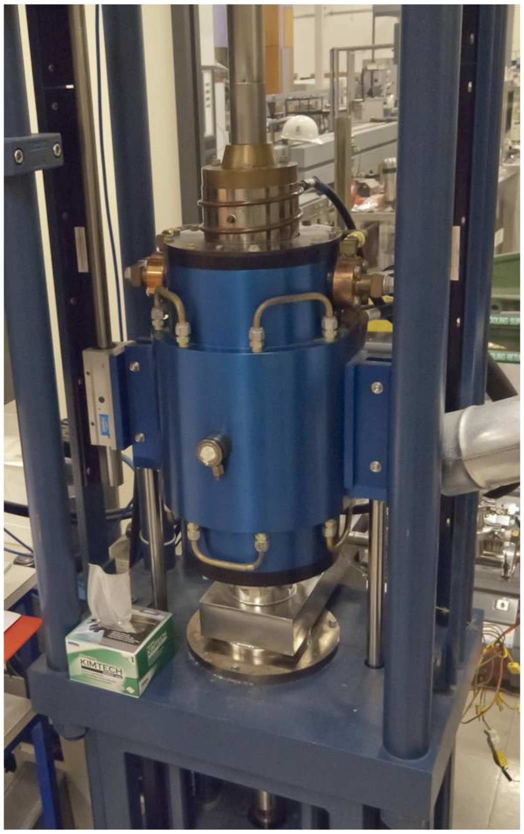

Figure 8. OSU diffusion welding furnace and ram assembly.

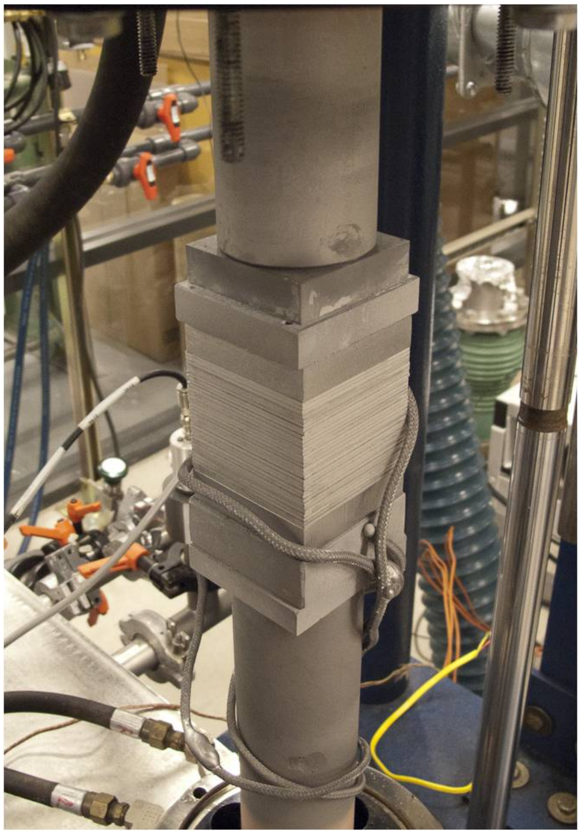

Figure 9. Diffusion weld stack of 800H and end plates before welding.

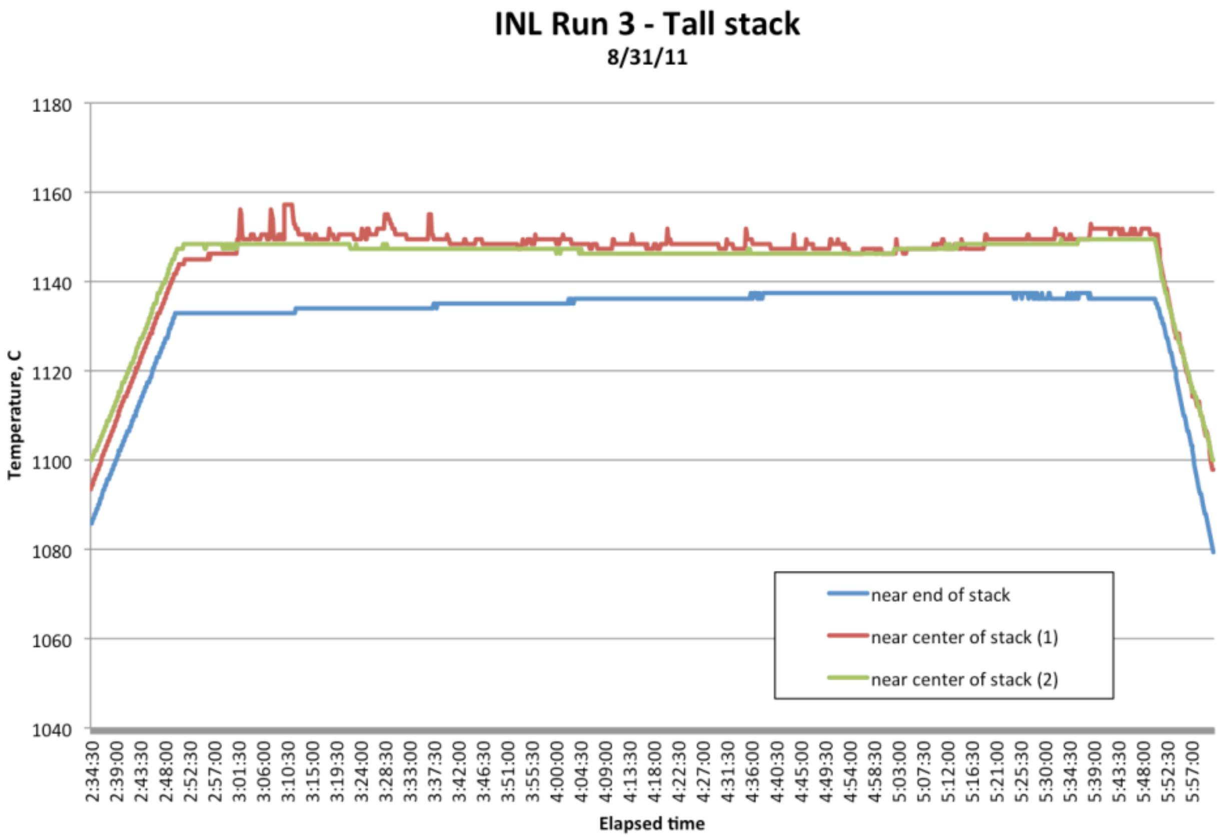

Figure 10. Temperature record for tall stack (23 sheets).

The two blocks that were successfully welded are shown in Figure 11. The block on the left will be referred to as the short stack (Samples 1-1A, 2A, and 3A) and the block on the right will be referred to as the tall stack (Samples 2-1A, 2A, and 3A).

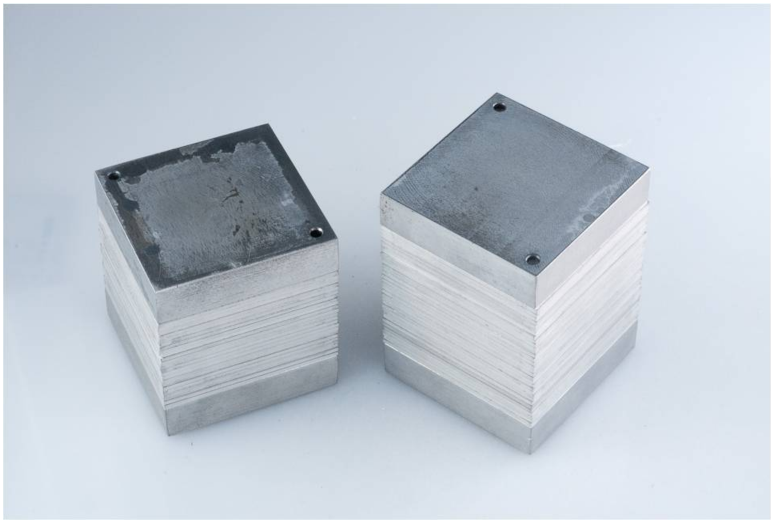

Figure 11. Alloy 800H diffusion welded test blocks.

The design of the test samples that will be removed from the two blocks for tensile testing and light optical and scanning electron microscopy are shown in Figure 12. The tensile test bars are the cylindrical sections and the metallography samples are highlighted in green. The tensile bars were machined to the requirements of ASTM E-8.

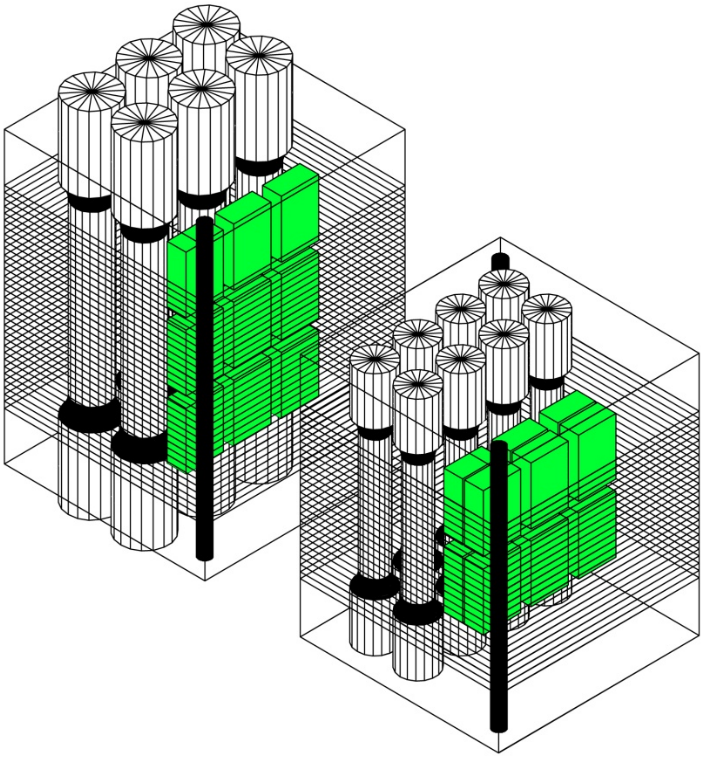

Figure 12. Test sample design.

2.3.3.3 Mechanical Properties Test Results

The as tested specimens are shown in Figures 13 and 14. All specimens show a flat fracture surface with limited indications of the necking which would correspond to a ductile fracture mode. All six specimens fractured at the same interface, indicating that that particular interface was the weak point in the stack, for a variety of possible reasons: a difference in the surface finish, cleaning, or plating of one or both metal surfaces at that interface layer. In addition, the specimens in the short stack showed failure or near-failure in the adjacent layer (in Figure 13, one layer went missing during the tensile testing of 1-2A, and incipient failure can be seen in 1-1A and 1-3A).

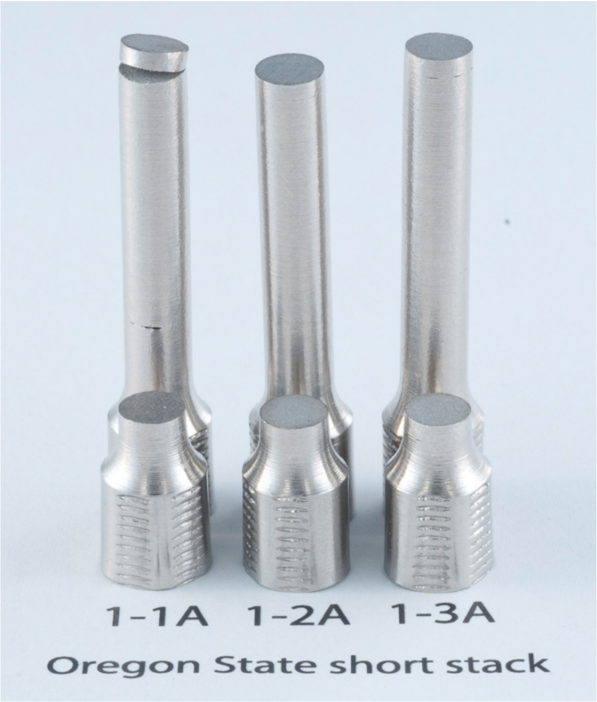

Figure 13. Tensile samples from short stack.

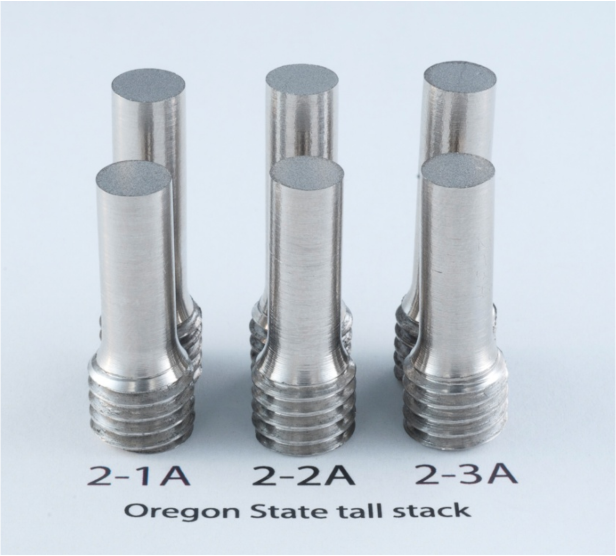

Figure 14. Tensile samples from short stack.

The ultimate tensile strength (UTS), yield strength, and ductility (reduction of area) of the specimens as shown in Table 6 was below that measured on the specimens welded on the Gleeble System. The earlier tests performed in the Gleeble had UTS values over 90% (~78 ksi) of the values of the bar base material used for the weld, and reduction of area values in the 65% range.

Table 6. Mechanical properties data.

Specimen ID	Ultimate Tensile Strength (ksi)	Yield Strength (ksi)	Reduction of Area (%)
Short stack average; % of base metal values	59.0; 75.7%		11.2;17.2%
1-1A	62.4	N/A	13.7
1-2A	52.4	N/A	7.7
1-3A	62.4	N/A	12.2
Tall stack average; % of base metal values	54.9; 70.3	31.8; ???	7.73; 11.9%
2-1A	50.9	31.5	5.8
2-2A	55.5	31.5	8.2
2-3A	58.2	32.5	9.2

Figure 15 is an optical photomicrograph showing two welds. The desired condition for a good diffusion weld is for grain growth across the interface and, essentially, the disappearance of the interface in the resulting microstructure; it can be seen that this did not happen. Figures 15A and 15B show a higher magnification views of these interfaces.

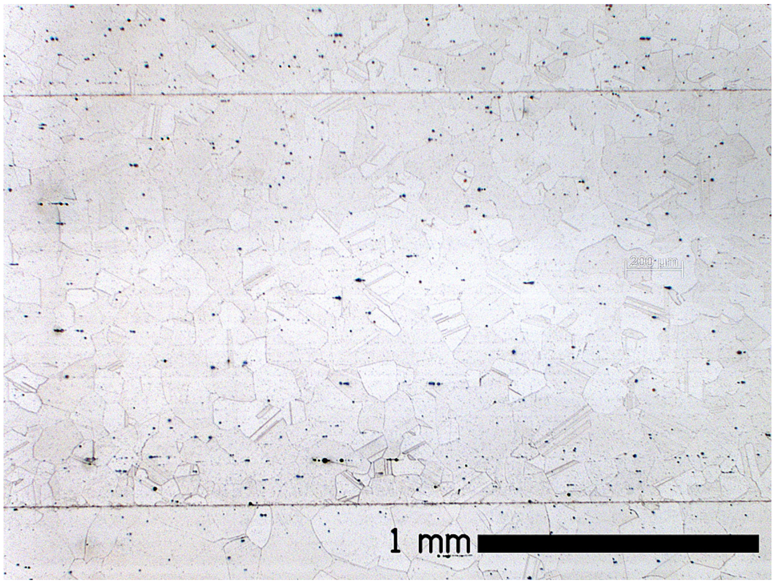

Figure 15A. Low-magnification optical photomicrograph of two welds in the middle section of the taller stack.

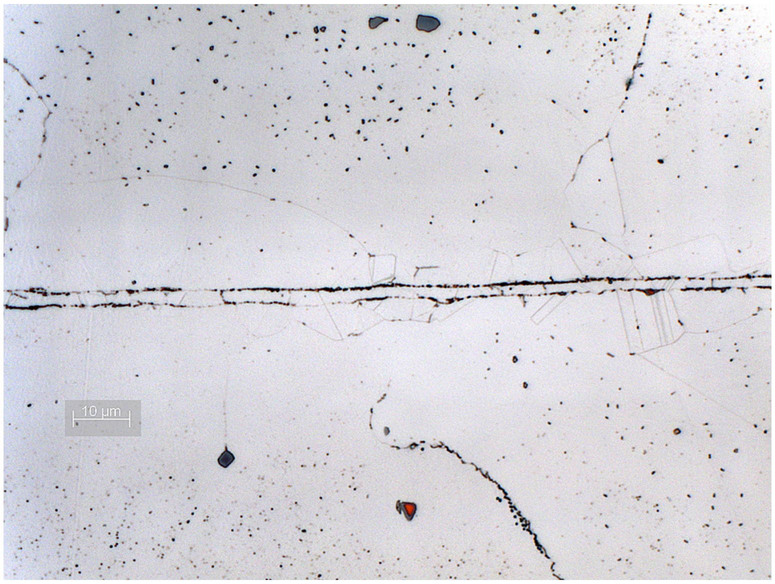

Figure 15B. Higher-magnification optical photomicrograph of a weld in the middle section of the taller stack.

The bond line illustrated in Figure 16 shows a lack of grain growth across the bond line with unbounded areas. Under these conditions, low mechanical property values might be expected.

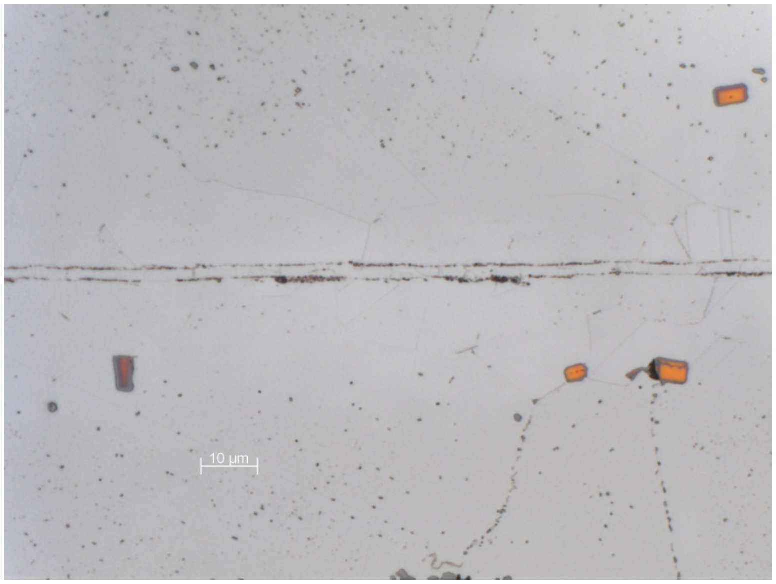

Figure 16. Diffusion weld bond line.

A possible explanation for these results is that the Gleeble System, welding a ½-in. diameter specimen, puts the bond interface in an approximately plane stress condition. which would allow more plastic flow at the interface. In addition, Gleeble specimens by nature have a thermal gradient from the control temperature at the bond line to water-cooled grips about 1.5 in. away; although the gradient is fairly flat near the bond line (as measured by secondary thermocouples placed during development), the existence of this cooler (hence higher-strength) material may further alter the stress state at the interface. The vacuum furnace/ram system at OSU, welding a 2.1-in. square specimen, places the bond line interfaces in an approximately plane strain condition (which tends to inhibit plastic flow). Both welding systems are effectively under load control, but these differences in geometry and state-of-stress may have an effect. Another possible explanation is that the vacuum furnace ram has a longer heating and cooling cycle than the Gleeble, leading to more of the cycle time being spent at temperatures just below the welding temperature, so that second phases not seen in the Gleeble may be apparent in the OSU specimens. Finally, there is fairly high confidence in the temperature measurement and control, and the degree of part mating or mismatch, in the Gleeble, partly because the joint and the control thermocouple are visible throughout the welding cycle. The OSU process, contained in a furnace, is not visible, increasing the chance of unobserved misalignment, thermocouple slippage, etc.

2.3.4 Scanning Electron Microscopy Results

Diffusion welding of three thin gage plate stacks (2.1-in. square stacks of 1/16-in.-thick 800H material with a 1-µM nickel plate on each faying surface) has been performed at OSU. The nominal welding conditions were 1150°C, three hours, vacuum, and an applied force of 5 MPa. The results of the initial light optical microscopy and mechanical property measurements were reported earlier. A scanning electron microscopy investigation has been completed on the three test stacks. Chemical composition measurements were performed on scan lines 35 µM in length.

Figure 17 shows the scan line for the sample that suffered a partial meltdown because of thermocouple failure. Figure 18 shows a scan line across a weld performed on one of the other stacks. What is interesting is that the chemical analysis shows a uniform chemical composition across the weld and evidence of titanium rich second phases present at the bond line. This has not been observed in the earlier diffusion welds made with the Gleeble System. Quantitative values for the elemental analysis shown in Figures 17 and 18 are presented in Table 7.

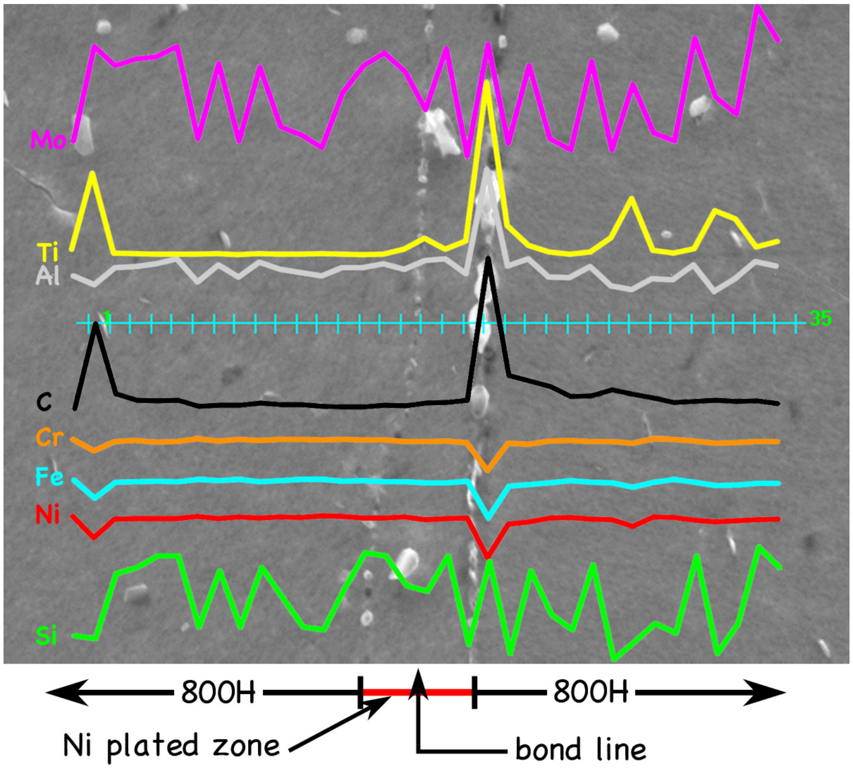

Figure 17. SEM chemical composition scan line – melted stack.

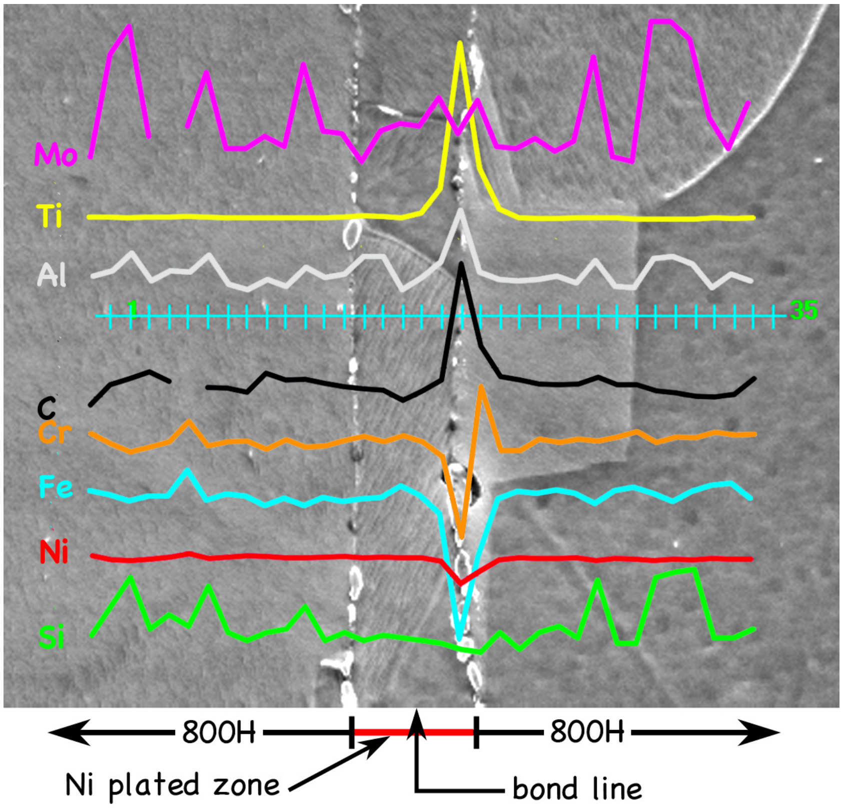

Figure 18. SEM chemical composition scan line – taller stack.

Table 7. Quantitative values for elemental analysis seen in Figure 16 and 17.

Position	Taller OSU-Welded Stack								Melted OSU-Welded Stack							
	C K	Al K	Si K	MoL	Ti K	Cr K	Fe K	Ni K	C K	Al K	Si K	MoL	Ti K	Cr K	Fe K	Ni K
1	1.74	0.74	0.51	0.21	0.39	19.99	42.38	34.05	1.32	0.71	0.46	0.27	0.66	20.46	44.08	32.03
2	2.42	0.77	0.61	0.61	0.39	19.75	42.21	33.23	6.08	0.61	0.45	0.72	5.16	19.04	39.58	28.36
3	2.64	0.87	0.71	0.72	0.37	19.57	41.96	33.16	2.15	0.81	0.67	0.63	0.44	20.18	43.55	31.58
4	2.86	0.71	0.53	0.29	0.40	19.68	42.17	33.35	1.77	0.82	0.69	0.66	0.40	20.33	43.70	31.64
5	2.54	0.77	0.58		0.40	19.79	42.15	33.77	1.75	0.85	0.73	0.67	0.39	20.11	43.79	31.71
6		0.76	0.54	0.33	0.42	20.26	43.20	34.49	1.77	0.91	0.73	0.72	0.37	20.21	43.61	31.68
7	2.34	0.86	0.68	0.54	0.39	19.71	41.99	33.49	1.44	0.64	0.49	0.28	0.37	20.52	44.20	32.06
8	2.30	0.69	0.52	0.24	0.37	19.80	42.24	33.82	1.50	0.84	0.68	0.64	0.41	20.29	43.96	31.68
9	2.17	0.66	0.49	0.24	0.35	19.82	42.16	34.10	1.51	0.70	0.49	0.27	0.36	20.47	44.19	32.00
10	2.82	0.72	0.52	0.29	0.36	19.62	41.76	33.92	1.64	0.87	0.69	0.62	0.40	20.31	43.65	31.82
11	2.58	0.68	0.53	0.25	0.35	19.84	42.08	33.70	1.54	0.79	0.59	0.34	0.39	20.45	43.94	31.96
12	2.60	0.79	0.61	0.57	0.37	19.68	41.76	33.62	1.55	0.75	0.49	0.30	0.38	20.44	44.16	31.92
13	2.48	0.73	0.49	0.31	0.36	19.71	42.10	33.82	1.43	0.71	0.48	0.24	0.41	20.43	44.16	32.14
14	2.36	0.75	0.52	0.30	0.40	19.83	41.94	33.92	1.40	0.81	0.62	0.50	0.37	20.46	43.82	32.02
15	2.29	0.85	0.49	0.19	0.45	19.92	42.06	33.75	1.42	0.81	0.74	0.63	0.35	20.41	43.89	31.76
16	2.24	0.85	0.51	0.31	0.42	19.79	42.09	33.78	1.50	0.85	0.73	0.69	0.39	20.39	43.70	31.75
17	1.90	0.66	0.50	0.34	0.36	19.93	42.57	33.73	1.47	0.79	0.63	0.60	0.68	20.18	43.66	32.00
18	2.22	0.73	0.49	0.33	0.59	19.80	42.19	33.65	1.62	0.89	0.61	0.42	1.33	20.22	43.37	31.54
19	2.59	0.82	0.48	0.44	1.84	19.46	41.43	32.94	1.65	0.91	0.73	0.71	0.67	20.28	43.42	31.65
20	6.53	1.12	0.46	0.30	9.23	17.62	36.37	28.38	1.78	0.74	0.43	0.20	1.16	20.09	43.83	31.75
21	3.73	0.76	0.45	0.43	2.86	21.06	39.73	30.98	9.77	1.95	0.71	0.73	10.52	16.63	34.76	24.94
22	2.70	0.72	0.52	0.25	0.81	19.60	42.06	33.33	3.18	0.83	0.40	0.26	2.06	19.99	42.57	30.72
23	2.59	0.71	0.46	0.24	0.36	19.60	42.34	33.70	2.86	0.91	0.68	0.63	0.89	19.89	43.01	31.12
24	2.44	0.72	0.52	0.28	0.33	19.86	42.27	33.58	2.57	0.70	0.53	0.28	0.52	20.27	43.39	31.74
25	2.43	0.74	0.54	0.23	0.31	19.78	42.41	33.56	2.00	0.69	0.48	0.23	0.38	20.35	43.98	31.88
26	2.44	0.70	0.50	0.27	0.34	19.86	42.26	33.64	2.03	0.82	0.70	0.65	0.51	20.20	43.52	31.58
27	2.67	0.83	0.70	0.60	0.34	19.81	41.85	33.19	2.37	0.60	0.38	0.23	1.36	20.22	43.33	31.51
28	2.42	0.68	0.48	0.21	0.34	19.91	42.38	33.59	2.13	0.55	0.44	0.54	3.67	20.02	42.31	30.34
29	2.43	0.67	0.48	0.19	0.30	20.03	42.53	33.37	1.90	0.68	0.50	0.31	0.60	20.51	43.56	31.94
30	2.22	0.84	0.71	0.74	0.29	19.78	42.27	33.15	1.65	0.67	0.47	0.27	0.43	20.46	44.21	31.86
31	2.14	0.85	0.73	0.74	0.29	19.90	41.95	33.39	1.72	0.84	0.73	0.76	0.70	20.28	43.55	31.42
32	2.03	0.81	0.74	0.67	0.28	19.89	42.34	33.24	1.79	0.53	0.40	0.48	2.93	20.01	42.74	31.12
33	2.00	0.67	0.50	0.36	0.36	20.01	42.60	33.50	1.73	0.68	0.50	0.40	2.47	20.09	42.85	31.27
34	2.10	0.75	0.50	0.24	0.31	19.95	42.67	33.47	1.75	0.88	0.76	0.91	0.80	20.17	43.20	31.53
35	2.62	0.71	0.53	0.42	0.34	19.96	42.08	33.35	1.61	0.83	0.69	0.75	1.13	20.20	43.22	31.58
Avg.	2.55	0.76	0.55	0.37	0.74	19.79	41.96	33.36	2.15	0.80	0.59	0.50	1.26	20.13	43.21	31.36
Heat Analysis	0.07	0.54	0.32	--	0.54	20.63	46.60	30.33	0.07	0.54	0.32	--	0.54	20.63	46.60	30.33

2.3.5 Scale-Up Issues

The diffusion welding process represents a complex combination of interatomic diffusion, plastic flow, which could possibly be accompanied by the redistribution of grain orientation and sizes. We need to introduce corrections for diffusion welding scale up that includes plastic deformation and flow phenomenon on nano, micro and macro scales.

An example of this is from development of chemical processes. From a chemical engineering design standpoint, we know that chemical reactors have characteristic times for chemical reactions and diffusion effects. Therefore, scale-up will depend upon the size of the reactor. Typically, in industry this is done via a number of adjustable coefficients and tedious experimentation.

To evaluate this effect, an elegant mathematical formalism exists called “similarity theory”. In the proposed research, we will make a research effort aimed at understanding plasticity phenomena in different diffusion welded components using the most advanced plasticity models and experimental data from scanning electron microscopy evaluations. We will also study the conditions in which one could avoid the formation of interlayer precipitation and elimination of porosity.

2.3.6 Thermodynamic Modeling using *Thermo-Calc*©

Before conducting any diffusion welding modeling, it was important to establish the equilibrium phase composition of Alloy 800H at all temperatures of interest, notably 1150°C. Indeed, higher temperatures will result in accelerated creep and creep-rupture of the samples, while at lower temperatures it would take too much time for thermally activated diffusion processes to proceed. Consequently, the temperature optimization hold point had to be determined based upon these factors, and an understanding of the appearance of other possible phases in the 800H microstructure incorporated as a function of temperature.

It is important to emphasize that this is not a systematic thermodynamic study of the complex 12-component plus 1 impurity system representing Alloy 800H. Rather, the goal was to understand the alloy’s phase composition as a function of temperature and the concentrations of its different components and, on that basis, to optimize the subsequent diffusion welding process. To achieve that goal, changes in the phase composition of Alloy 800H were plotted as a function of temperature, as shown in Figure 19.

This “phase composition – temperature” property diagram demonstrates that in a temperature range of 800 to ~1320°C, the microstructure of Alloy 800H is defined by the austenitic matrix and a relatively small amount of the mixed titanium and niobium carbonitrides. These are constituent particles that disappear only at temperatures above ~1320°C, followed by melting of the Alloy 800H beginning at ~1360°C. Within the broad temperature range of 800 to ~1300°C, the volume fraction of the [(Ti, Nb)(C,N)] particles remains small (less than 0.5%). It follows from a single equilibrium calculation at 1150°C that the concentration of niobium in these constituents was ~10 times higher than in the fcc matrix, and nitrogen is higher by 4 orders of magnitude in the fcc matrix.

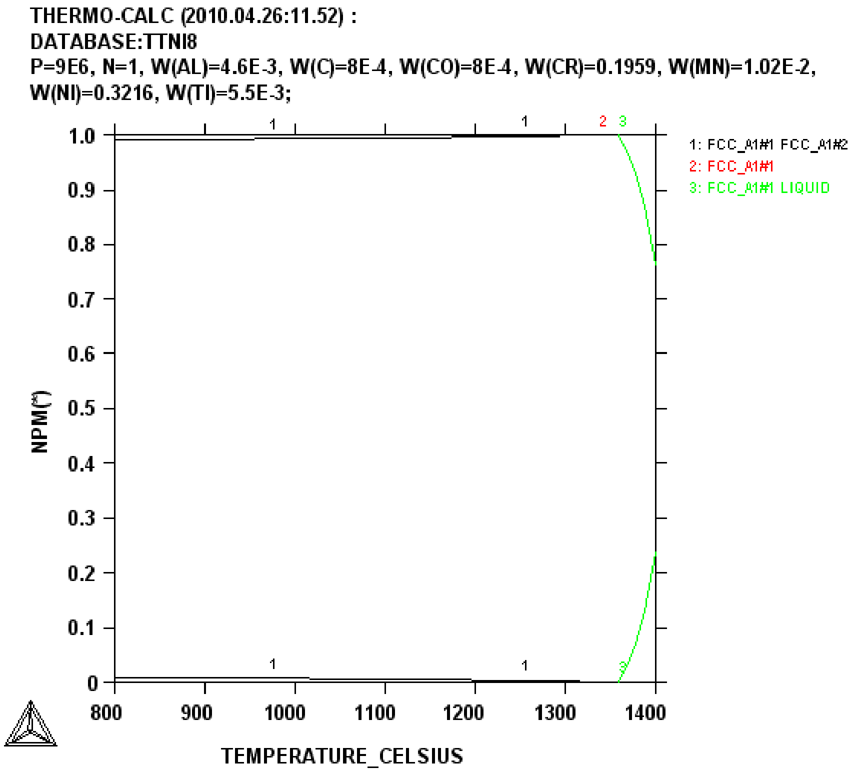

Figure 19. Phase composition of Alloys 800H as a function of temperature.

The chemical composition of the several carbonitride particles established using energy-dispersive x-ray spectroscopy (EDX). Imaging of these secondary phases with the SEM is shown in Figure 20. The particles present in microstructure, in agreement with thermodynamic calculations, are [(Ti, Nb)(C, N)]. Chemical compositions of the particles, according to the results of EDX analyses, are as follows (all in at %): Particle 1: C-30.3, N-12.6, Ti-40.4, Nb-5.7, Fe-4.6, Cr-2.9, Ni-2.8, and Mo-1.25; Particle 2: C-36.5, Ti-42.4, Nb-11.7, Fe-3.2, Cr-2.7, Ni-1.7, and Mo-1.7.

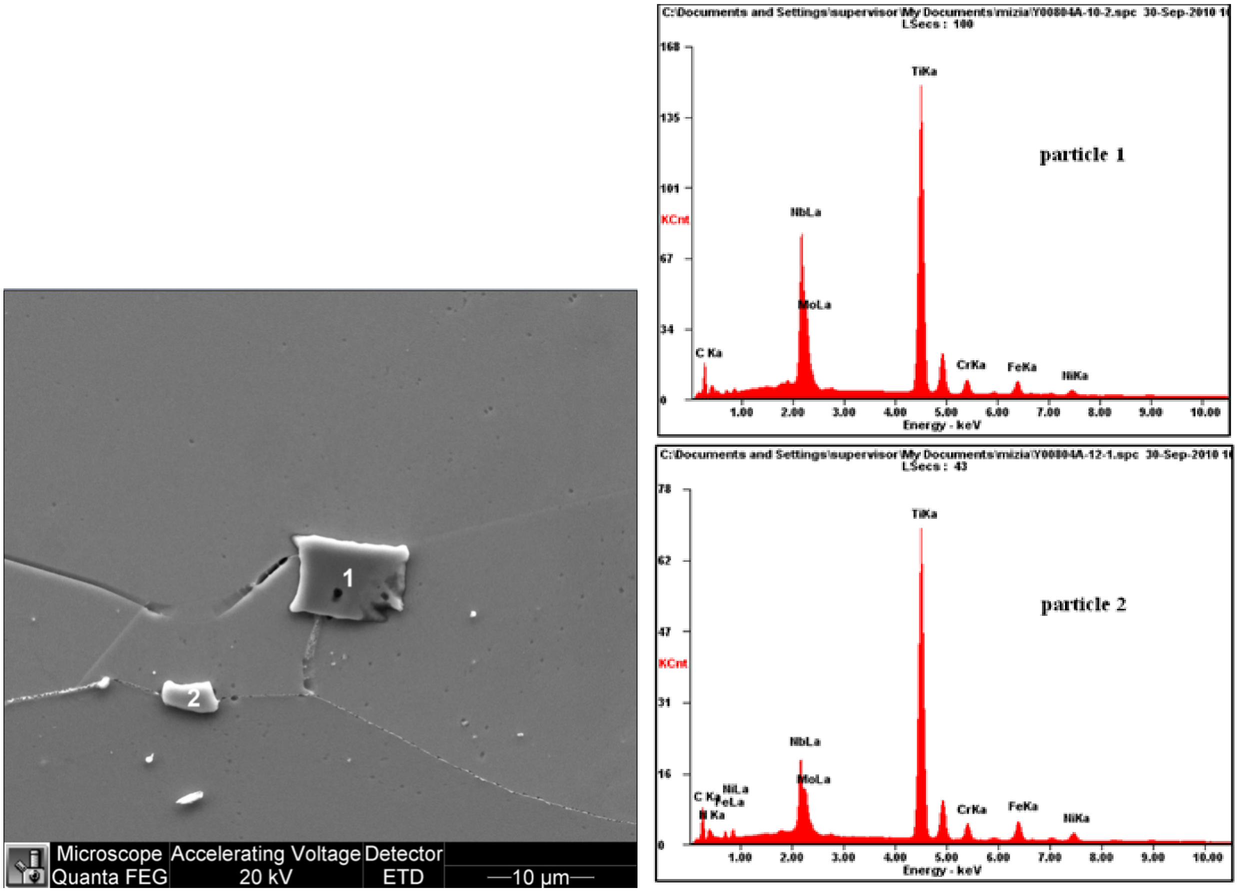

Figure 20. SEM image of an Alloy 800H sample heat treated at 1150°C for 3 hours and then quenched to room temperature.

The presence of 0.053 wt% niobium and 0.007 wt% nitrogen in Alloy 800H samples was something of a surprise, as these elements are not listed in the ASTM International specification for this alloy. However, because superalloys are often recycled, one should expect that small amounts of such tramp elements could nevertheless be present. Such impurities are typical of real alloys and can be a complicating factor in accurate modeling.

All subsequent thermodynamic calculations were made under the assumption that the niobium concentration in the studied alloy was zero. This was done to expedite thermodynamic calculations and also to make the modeled diagrams less overburdened with different phase domains. The concentration of nitrogen, as measured and reported in Table 1, was taken as 0.07 wt%.

The introduction of niobium into the computations at temperatures above 800°C results in the formation of a mixed compound [(Ti,Nb)(C,N)], with practically all niobium entering the composition of these constitutive particles (see above). As temperature decreases, the D0$_{22}$–superstructure (Ni$_3$Nb) can be formed in addition to the L1$_2$ superstructure (Ni$_3$Ti)[c]. In the literature,[2] these compounds are called the γ’’- and the γ’-phases, respectively. The locations of phase equilibrium boundaries (e.g., the precipitation of M$_{23}$C$_7$) can also be shifted in the “temperature – concentration” figurative space of the diagram.

---

[c] *Structurbericht* designation *L12* corresponds to the Pearson symbol *cP4* with prototype Cu3Au; while the *D022* designation – to the Pearson symbol *tI8* with prototype TiGa3.

Among other phases found in Alloy 800H, it is important to mention the sulfur-bearing particles that were observed.[19] For this reason sulfur was included in thermodynamic calculations, even though this impurity's concentration in 800H was very small, 0.001 wt% sulfur. As it follows from the carbon isopleth analysis shown in Figure 21, it was indeed established that such compounds as manganese sulfide, titanium carbosulfide, $Ti_4C_2S_2$, and pyrrhotite (containing titanium, manganese, sulfur, and other elements) could be found in 800H, in agreement with experimental results.[19]

There have been numerous research efforts aimed at the microstructural characterization of Alloy 800H under different heat treatment conditions,[20,21] so the general understanding of the alloy microstructure problem achieved during the last 30 years is very good. However, the thermodynamics modeling work for such complex materials that would reconcile and explain the phase equilibria and thermodynamic data is practically absent. This was yet another rationale for undertaking the present work.

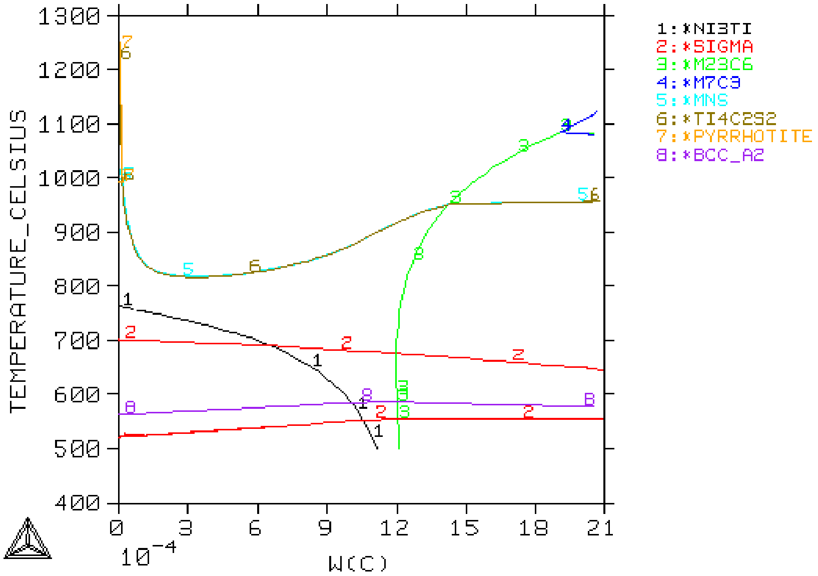

Figure 21. Carbon-isopleth for Alloy 800H.

An interesting feature of the carbon isopleth in Figure 21 is the appearance of the sigma phase (a bcc intermetallic compound containing iron and chromium). The red lines correspond to the appearance and disappearance of the sigma phase. As can be seen, the two elements can be in equilibrium with a bcc phase representing solid solutions of chromium in iron. To better understand the nature of these equilibria, the binary iron-chromium phase diagram was reviewed and is shown as Figure 22. It was calculated using the software and databases indicated above.

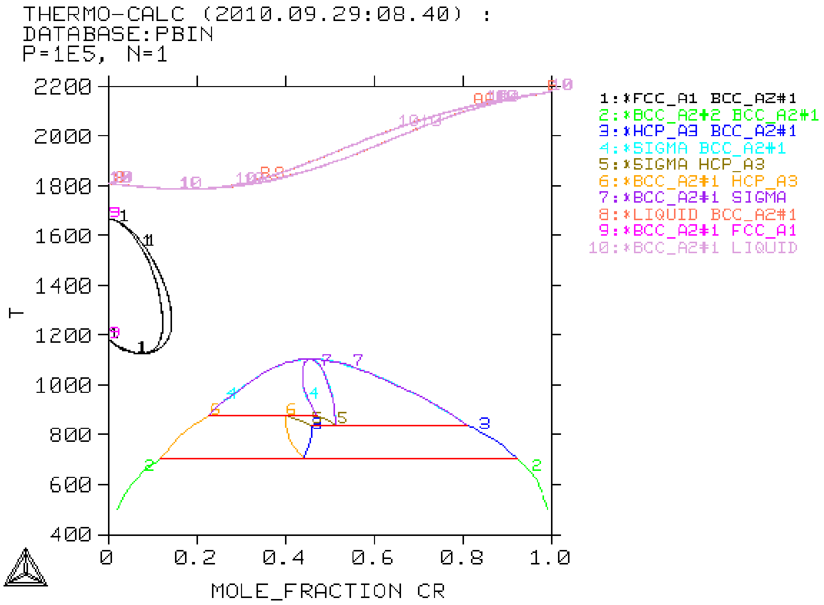

Figure 22. Iron-chromium phase diagram for Alloy 800H.

The iron-chromium phase diagram in Figure 22 is characterized by miscibility gap in the solid state. The sigma phase can be in equilibrium with iron-chromium and chromium-iron solid solutions—lines 7 and 4. This suggests that the appearance of the bcc phase on the diagram was related to the miscibility gap. This assumption was checked by constructing the chromium-isopleth shown in Figure 23.

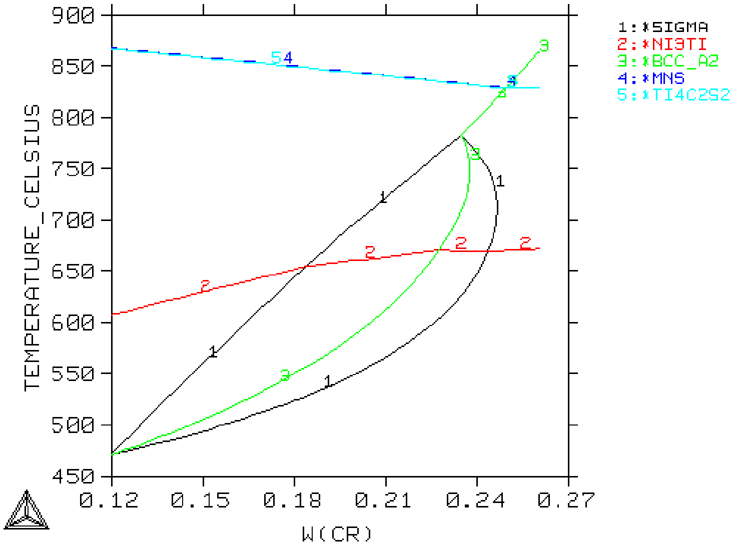

Figure 23. Chromium-isopleth for Alloy 800H.

It is obvious in Figure 23 that all three branches corresponding to the sigma phase at ~770°C, coalesce, below the miscibility gap at ~475°C, into a single phase again. Consequently, according to the model, the potential appearance of a small amount of bcc chromium-iron solid solution in the fcc matrix accompanying the formation of the sigma phase is to be expected.

Overall, the relatively narrow temperature range of ~800 to 450°C should be treated with extreme caution, as a number of different phases may precipitate from the austenite fcc-solid solution matrix when exposed to this temperature range for a sufficient length of time. In particular, this information needs to be taken into account when evaluating welding regimes for Alloy 800H and similar materials such as cooling diffusion-welded samples from 1150°C to ambient temperature. Although the Gleeble is capable of relatively rapid cooling through this range, processes commonly used for the fabrication of actual components may not be able to achieve this. Phases formed in this lower temperature regime may also be an issue in service.

The titanium-isopleth shown in Figure 24 demonstrates convincingly that, for the selected concentrations of nickel and titanium—32.16 and 0.46 wt%, respectively—as well as other chemical elements in 800H, the phase field comprising the fcc matrix and [(Ti,Nb)(C,N)] constituents exists in a very broad range of temperatures; the same range that was established from the property "step" diagram in Figure 19.

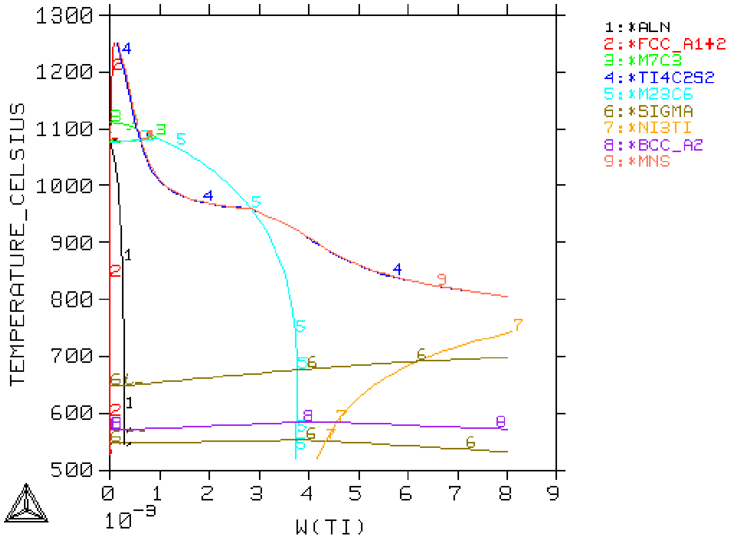

Figure 24. Titanium-isopleth for Alloy 800H.

Again, the principal thrust of this work was not aimed at studying complex phase equilibria in 12-component superalloys, but rather, to get useful information for the simulation of the diffusion welding process of components made of such alloys. This work, both experimental and modeling, is described below.

2.3.7 *Dictra* Modeling of the 800H/Ni/800H Diffusion Couple, Comparison to Experiment, and Optimization of Welding Conditions

Dictra is a versatile tool for studying practically all of the diffusion controlled phenomena in metallurgical systems. In particular, diffusion couples of different types (I, II, or III, according to the classification proposed by Morral, Jin, Engstrom, and Agren[22] and Hopfe and Morral[23,21]) may undergo a cascade of phase transformations at the interface while reducing the chemical potential gradient of the system and approaching equilibrium. The present work is limited to the construction of concentration profiles for the principal alloying elements in the Alloy 800H specification (iron, chromium, and nickel) in contact with nickel. In order to accelerate the already slow process of computing diffusion processes in an 11-component Alloy 800H, it was decided at the first stage to ignore the evolution of the [(Ti, Nb)(C, N)] constituent particles' spatial distribution.

The concentration profiles modeled using the techniques described in Section 2 are presented in Figure 25. It can be seen that in the case of the three major elements in Alloy 800H (chromium, iron, and nickel) that there is a reasonable degree of agreement between the results of calculations and experimentally measured (EDS) concentration profiles. Similar results were obtained for all other chemical elements. This suggests that the original assumptions (ignoring [(Tι, Nb)(C, N)]-constituents) were reasonable, and the quality of the thermodynamic and mobility data bases used was adequate.

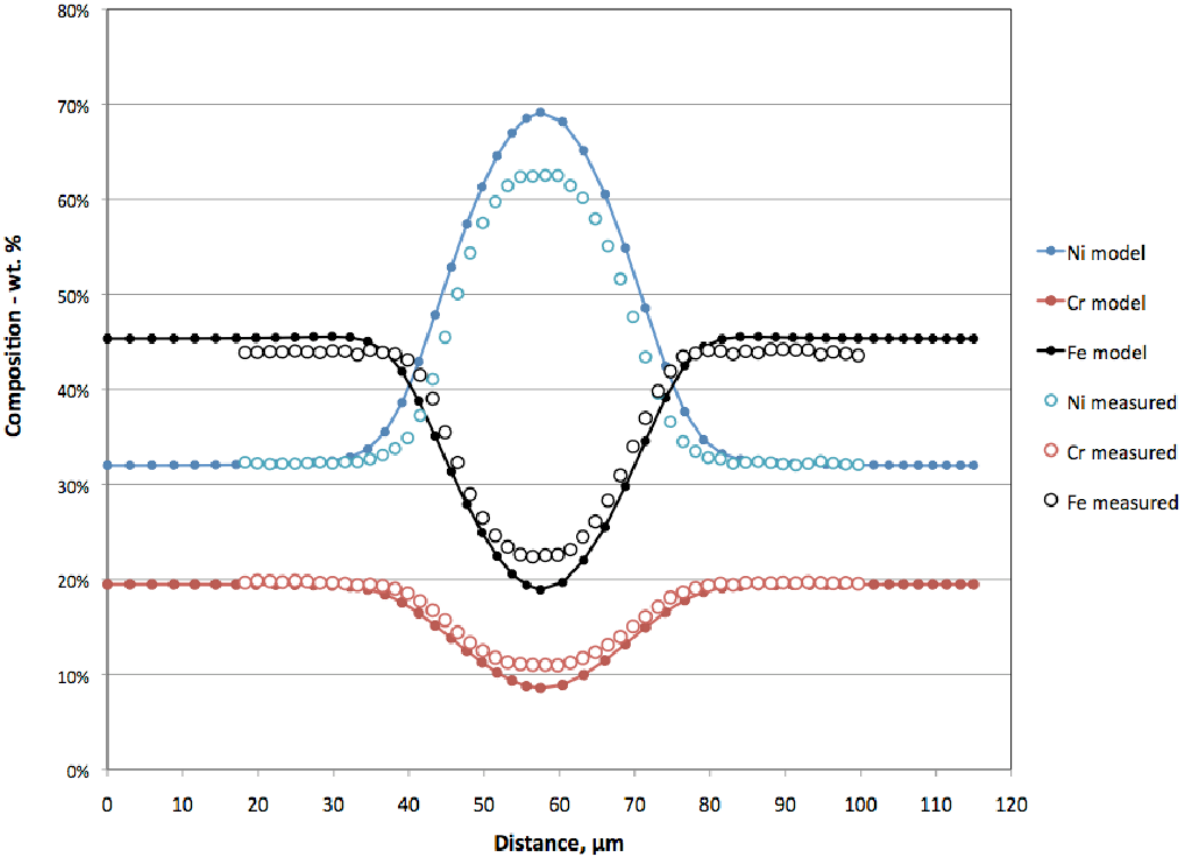

Figure 25. Comparison of model and experimental data (SEM/EDS analyses) for diffusion bonded specimen comprised of Alloy 800H (15 µm of nickel foil filler) and Alloy 800H. The duration of process was 3,600 sec at compressive pressure of 5 MPa and temperature 1150°C. *Dictra* modeling was done for the same conditions.

The quantitative agreement between the results of modeling and experiment is not complete. Indeed, all modeling results, especially in the vicinity of the concentration profile extreme, demonstrate consistently that the modeled estimates correspond to somewhat slower diffusion taking place in the modeled system. This might be caused by minor imperfections of the existing mobility databases and the need for some minor adjustments (to be done later), or by an inability to measure the concentrations of light elements reliably (C, N), thus causing some errors in the assessment of the effective concentrations of iron and other elements; or both. Nevertheless, the trends in all cases have been captured correctly and provide a solid basis for understanding diffusion welding processes in complex systems.

The results obtained for 2 and 3 hours at 1150°C, as well as for welding at temperatures of 1000°C, were less satisfactory because the conditions listed here (1500°C, 3,600 sec (1 hour), 5 MPa) achieved a chromium concentation of 12 wt%, in the nickel foil bond interface area. This gives the nickel interlayer area additional strength and corrosion resistance, as well as keeping process time relatively manageable.

Although further testing must be done, particularly of the mechanical, corrosion, and other properties of these joints, *Thermo-Calc*/*Dictra* modeling has indicated useful directions for paring down the actual test matrix, evaluating different interlayer thicknesses (or even different interlayer materials), and other tasks in progress towards a welding specification for this alloy.

2.4 ASME Standards Development

The IHX is a component that will need to be qualified to the requirements of the American Society of Mechanical Engineers Boiler and Pressure Vessel (ASME BPV) Code, Section III, Division 5,[24] which currently has no rules for construction of diffusion welded compact heat exchangers. A diffusion welding procedure and performance qualification standard has been developed for ASME Section IX, "Welding and Brazing Qualification,"[25] The requirements for the fabrication, tensile testing, and microstructural evaluation of 8 × 8 × 8 in. test blocks are given in Paragraph QW-185. Paragraph QW-250 describes the requirements for the welding variables used for weld procedure specification qualification. Welding variables needed to qualify a welding procedure specification for diffusion welding are presented in QW-266, "Welding Variables Procedure Specifications Diffusion Welding" and listed in Table 8.

Table 8. Welding variables needed to qualify a welding procedure specification for diffusion welding.

Paragraph		Brief of Variables	Essential	Supplementary Essential	Nonessential
QW-403 Base Metals	.28	Base metal grade	X		
	.29	Ø Surface finish	X		
QW-404 Filler Metal	.53	+ Filler metal and composition	X		
QW-407 PWHT	.10	+ PWHT temperature, time, cooling rate	X		
QW-408 Gas	.25	Ø Furnace Atmosphere	X		
QW-410 Technique	.70	Ø Preassembly Cleaning	X		
	.71	< Block Compression	X		
	.72	< Welding time or temperature	X		

Legend:
+ Addition > Increase/greater than ↑ Uphill ← Forehand Ø Change
- Deletion < Decrease/less than ↓ Downhill → Backhand

Current ASME Code rules for Section VIII, Division 1 fabrication of microchannel heat exchangers are described in Code Cases 2437-1[26] and 2621-1.[27] It should be noted that the approved materials listed in Code Case 2621-1 for 304L(UNS S30403), 316L(UNS 31603), and 2205 Duplex (UNS S31803) may not be appropriate choices for diffusion welded compact heat exchangers for application in nuclear assisted, high temperature industrial processes.

3. SUMMARY

The results of this work indicate that a filler metal is needed for diffusion welding to achieve good grain growth across the joint, resulting in acceptable mechanical properties. The method of application (nickel foil or nickel plating) will need additional optimization work.

The issue of the required vacuum level needs further investigation. Some data show that an overnight pump-down in the Gleeble system achieves a better vacuum, resulting in less surface oxidation and, in one case, mechanical properties equaling those obtained with a filler metal addition.

The thermodynamic and diffusion modeling work presented in this paper pursued two interdependent goals. First, to verify that the methods of diffusion modeling implemented in *Dictra* and the corresponding databases for superalloys—TTFE6 (TTNI8) and MOBFE1 (MOBNI1)—can quantitatively describe the real diffusion couples made of Alloy 800H and nickel foil filler metal with confidence. Second, to use these tools to predict the optimal conditions for diffusion welding of 800H.

Experimental results on concentration profiles of different chemical components in Alloy 800H (obtained using EDS) match the model reliably. Additional work needs to be done to understand the nature of some discrepancies, especially in the center of the nickel interlayer. After the fundamental work of Campbell et al.,[8] it became clear that very complex multicomponent heterogeneous alloys could be modeled using *Dictra*. The present work was conducted in order to verify that these tools will serve reliably for the modeling of diffusion welding. This goal was achieved, and the modeling and optimization of diffusion welding for similar and/or dissimilar materials can proceed with confidence.

The second goal was to optimize the welding conditions and reduce the number of experiments. This goal was only partially achieved (established an optimal temperature and time of welding to be 1 hour at 1150°C). Further work is necessary to account for heat-up schedules, plasticity, and creep effects at the process temperature. This will be done using optical imaging microscopy and crystallographic texture analyses, which will be coupled to state-of-the-art plasticity models for this type of material.

The diffusion welding process represents a complex combination of interatomic diffusion and plastic flow. We need to introduce corrections for diffusion welding scale from from the small scale Gleeble sample preparation to fabrication of palte arrays that includes the study of plastic deformation and flow phenomenon on nano, micro and macro scales.

4. CONCLUSIONS

Models of diffusion welding in 800H with a nickel foil interlayer accurately predicted diffusion profiles and provided a quantitative basis for developing experimental matrices. This work demonstrates the applicability and effectiveness of modern thermodynamic and kinetic computational tools that could be used to address many problems in modern physical metallurgy.

Experimentally optimized diffusion welding parameters were able to produce 90+% ultimate tensile strengths in 800H diffusion welds, with good ductility, indicating that the material can be fabricated into compact heat exchangers for further testing and development.

Techniques were developed for 800H that can also be applied to other candidate materials for NGNP IHX applications, such as Alloy 617.

5. RECOMMENDATIONS

1. Investigate additional surface conditioning treatments to achieve a better surface finish.
2. Investigate temperature control systems for the OSU system that accurately characterize the temperatures at the bonding surfaces.
3. Investigate producing corrections for diffusion welding scale from the small scale Gleeble sample preparation to fabrication of plate arrays that includes the study of plastic deformation and flow phenomenon on nano, micro and macro scales.
4. Characterize short-term diffusion phenomena (the Gleeble is ideal for this) for a finer time resolution, and use TEM for a finer spatial resolution and more accurate phase identification, leading to a more complete phenomenological model of the diffusion welding process.
5. Investigate the use of a thicker nickel plate on the faying (bonding) surfaces or use the nickel foil insert for the filler metal used in the joint.
6. Investigate stress state effects at the weld interface for both planar test assemblies and hypothetical multilayer plates containing channels typical of compact heat exchangers.

6. REFERENCES

1. J. N. Dupont, J. C. Lippold, and S. D. Kiser, *Welding Metallurgy and Weldability of Nickel-Based Alloys*, John Wiley and Sons, Hoboken, NJ, 2009.
2. M. J. Donachie and S. J. Donachie, *Superalloys – a Technical Guide*, 2nd edition, ASTM International, Metals Park , OH, 2002.
3. M. G. Nicholas, *Joining Processes - Introduction to Brazing and Diffusion Bonding*, Kluwer Academic Publishers, Dodrecht, 1998.
4. C. F. Jeff Wu and Michael S. Hamada, "Experiments: Planning, Analysis, and Optimization," *Wiley Series in Probability and Statistics*, Wiley, NY, 2009.
5. PLN-3565, "Scoping Investigation of Diffusion Bonding for NGNP Process Application Heat Exchangers," Revision 0, Idaho National Laboratory, July 8, 2010.
6. Idaho National Laboratory, "Next Generation Nuclear Plant Project Technology Development Roadmaps: The Technical Path Forward," INL/EXT-08-15148, Revision 0, January 2009.
7. N. Saunders and A. P. Miodownik, *CALPHAD (Calculation of Phase Diagrams): A Comprehensive Guide*, Oxford and New York, Pergamon, 1998.
8. M. Hillert, *Phase Equilibria, Phase Diagrams, and Phase Transformations*, Cambridge University Press, Cambridge (2007).
9. Zi-Kui Liu, "A Materials Research Paradigm Driven by Computation," *JOM*, October 2009, pp.18-20.
10. C. E. Campbell, W. J. Boettinger, and U. R. Kattner, Acta Mater., Vol. 50, 2002, pp.775–792.
11. Z. -K. Liu and L. -Q. Chen, *Applied Computational Materials Modeling: Theory, Experiment, and Simulations*, ed. By G. Bozzolo, New York, Springer, 2006, pp.171–213.
12. J. -W. Yoon, F. Barlat, H. Weiland, M. V. Glazoff, and R. E. Dick, *State of the Art For Crystal Plasticity Based Modeling*, Alcoa Technical Report No. 07-201, 2007. See also: M. V. Glazoff, S. N. Rashkeev, Yu. P. Pyt'ev, J. -W. Yoon and S. Sheu, *Appl. Phys. Letts*, Vol. 95, 084106, 2009.
13. ASTM B 408-06, "Standard Specification of Nickel-Iron-Chromium Alloy Rod and Bar," ASTM International, West Conshohocken, PA.
14. ASTM E-8/E8M-09, "Standard Testing Methods for Tension Testing Metallic Materials," ASTM International, West Conshohocken, PA.

15 C. Cabet and R. N. Wright, "Corrosion of Intermediate VHTR Heat Exchanger Alloys: Achievements of the US-France I-NERI Program," Paper No. 10226, Corrosion 2010, NACE International, Houston, TX, 2010.

16. ThermoCalc Software AB, *Thermo-Calc Classic Version S User's Guide*, Pingfang Shi and Bo Sundman, ed., Stockholm, Sweden, 2010.
17. DICTRA Version 25 User's Guide, *Thermo-Calc* Software AB, Stockholm, Sweden, 2010.
18. A. Borgenstam, A. Engstrom, L. Hoglund, and J. Agren, *Journal of Phase Equilibria*, Vol. 21, No. 3, 2000, pp.269–280.
19. A. A. Tavasoli and G. Colombe, *Metallurgical Transactions A*, Vol. 9A, 1978, pp.1203–1211.
20. X. Wang, E. Brunger, and G. Gottstein, *Materials Science and Engineering A*, Vol. A290, 2000, pp. 180–185.

21. A. Czyrska-Filemonowicz and K. Spiradek, Z. Werkstofftechnik, Vol. 14, 1983, pp. 417–421.
22. J. E. Morral, C. Jin, A. Engstrom, and J. Agren, *Scripta Materialia*, Vol. 34, Issue: 11, 1996, pp. 1661–1666.
23. W. D. Hopfe and J. E. Morral, *Acta Metallurgica et Materialia*, Vol. 42, Issue 11, 1994, pp. 3887-3894.
24. 2010 ASME Boiler & Pressure Vessel Code, Section 111, Division 5. “High Temperature Reactors” 2011 First Issuance, November 1, 2011
25. 2010 ASME Boiler & Pressure Vessel Code, Section IX: “: Qualification Standard for Welding and Brazing Procedures, Welders, Brazers, and Welding and Brazing Operators,” 2011 Addenda, July 1, 2011.
26. ASME Boiler and Pressure Vessel Code Case 2437-1, “Rules for Diffusion Bonded, Flat Plate, Microchannel Heat Exchanger,” Section VIII, Division 1, Approved June 23, 2005.
27. ASME Boiler and Pressure Vessel Code Case 2621-1, “Diffusion Bonding,” Section VIII, Division 1, Approved December 14, 2009.